EasyChair Preprint

№ 10214

Improving the Method of Linear-Quadratic Control over a Physical Model of Vessel with Azimuthal Thrusters

Vitalii Budashko

May 19, 2023

Improving the method of linear-quadratic control over a physical model of vessel with azimuthal thrusters

Vitalii Budashko

The object of this research is the algorithms for controlling large-scale models of sea-based vehicles (SBVs). The subject of the research is a linear-quadratic method for controlling a model of the propulsion complex with azimuthal thrusters (ATs) in the aft part. The problem is the solution between the interdependent throws of surge, sway, and yaw speeds predicted by the linear controller. Input signals are the rotational speeds and the angles of ATs propeller thrusts with respect to the diametrical plane of SBVs. During the simulation, step responses of a closed system for overload and rotation speed are compared. Simulation of speed jumps showed an adequate response, in contrast to the speed of rotation of ATs, which showed a greater impact on the system than the orientation of ATs. When modeling the rate of yaw, the behavior of the ATs angle did not correspond to its limitations inherent in the device rotating at the appropriate speed. It is concluded that this is the result of linearization of the actuators, and the proposed solution is to implement the strengthening of the task to better adapt to the rotating behavior of ATs. Despite these problems, the simulation showed the potential of the model and controller for use in similar situations. Several modifications are also offered to significantly improve the model and simulations. One of the main changes that could be made is the implementation of a predictive gain during the linearization of the ATs control system. The practical significance of the results obtained is the fact that the quadratic optimization model is an effective and reliable technique in the process of designing SBVs of various configurations of steering devices for optimal control

Keywords: modeling, thruster, linear-quadratic regulator, optimization, combined propulsion complex, dual purpose

1. Introduction

Azimuthal thrusters (ATs) reflect a growing trend in the modern market of sea-based vehicles (SBVs). AT is a propeller mounted in a nacelle under the body of SBV. This nacelle is able to rotate around its axis, which makes it possible to change the direction of the force acting on SBVs [1–3].

Unlike SBVs with ATs, most modern vessels are driven by a mechanical system with an internal combustion engine (ICE) or a propeller electric motor (PEM), which rotates the propeller through the shaft line system. The direction of rotation of the propeller is usually fixed relative to the hull of the vessel, and the control is carried out mainly by the steering pen in the aft. Some vessels also have tunnel thrusters (TTs) installed in the bow or aft parts that provide a lateral thrust to improve maneuverability capabilities, such as mooring. Another method of movement and maneuvering that is currently being used is ATs.

With greater maneuvering capabilities, there are more algorithms to control Ats located in the aft part, which require greater operator qualification, or a more complex

control system. The controller uses estimates of linear and angular velocities obtained using the Global Positioning System (GPS) and inertial measuring units (IMU) to control SBVs.

Therefore, research on the development of algorithms for controlling large-scale models of SBVs, based on the linear-quadratic principle of controlling thrusters, is relevant.

2. Literature review and problem statement

This research investigates how adequately it is possible to control a smaller vessel with ATs using a linear-quadratic regulator (LQR). This will require mathematical modeling of both the behavior of SBVs and the thrust pattern of propellers. Since LQR requires linear models for design, some simplifications and linearization will be needed. Thus, a linearized model will also be implemented to describe the movement of this type of SBV. The scale model of the SBV to be controlled is shown in Fig. 1.

In the AT model (Fig. 2), PEM is placed in a nacelle, which is installed under the body in such a way that it can rotate around a vertical axis. The propeller is driven by a mechanical transmission that connects it to the engine inside the vessel or to the PEM installed inside the nacelle itself. This structure eliminates the need for steering and provides better maneuverability of the vessel under compressed sailing conditions [4].

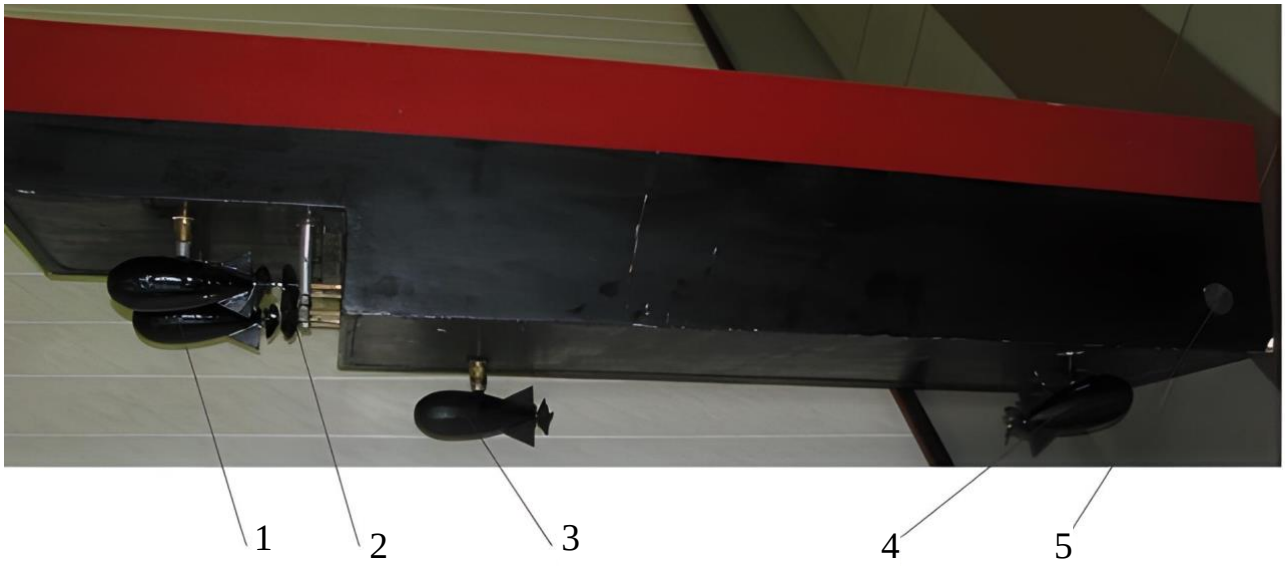

Fig. 1. General view of the physical model of a multifunctional propulsion complex with a variable structure: 1 – thruster of the *Contra–rotating propeller* system*;* 2 – main electric motor of the *Contra–rotating propeller* system; 3 – aft thruster; 4 – bow thruster with two degrees of freedom; 5 – bow tunnel thruster

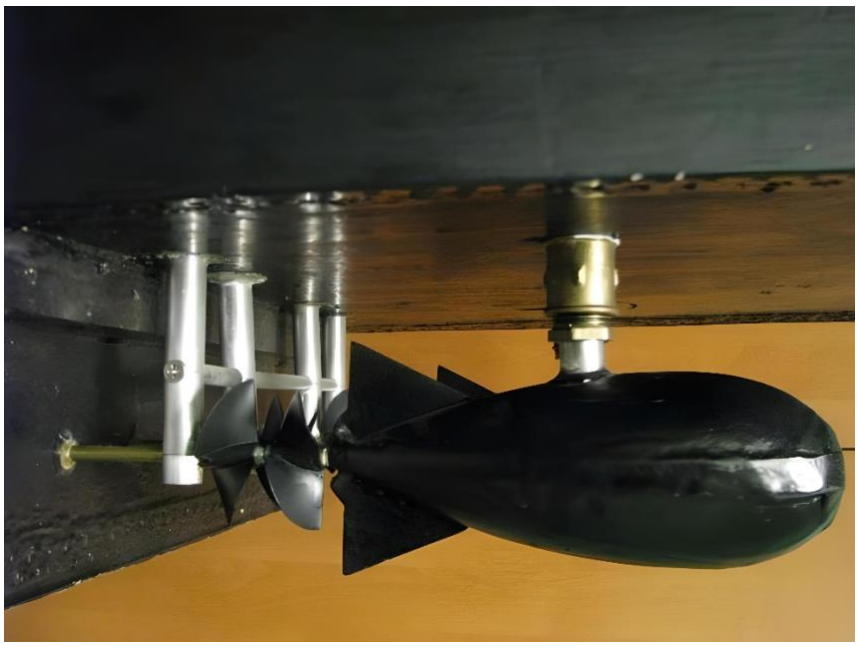

Fig. 2. General view of the physical model of azimuthal thrusters located in the aft part of the physical model of a multifunctional propulsion complex with a variable structure

To determine the SBV position, orientation, and speed of movement, appropriate movable and fixed coordinate systems are required. The most common representation for a fixed coordinate system is based on hull symmetry around the X_bZ_b-plane, approximate symmetry around the Y_bZ_b-plane, and projection onto the Z_b-axis relative to the surface of the water. The inertial (fixed) coordinate system is used to describe the position and orientation of the vessel in global coordinates and Euler angles as $[x\ y\ z]^T$ and $[\phi\ \theta\ \psi]^T$, respectively. The moving coordinate system describes forces, torques, linear velocities, and angular velocities $[X\ Y\ Z]^T$, $[K\ M\ N]^T$, $[u\ v\ w]^T$, $[x\ y\ z]$, and $[p\ q\ r]^T$, respectively. The movement of the vessel can be described by six degrees of freedom, which are divided into two categories. Translational motion in three directions: longitudinal movement (surge), transverse movement (sway), and vertical movement (rise), as well as rotational movement around three axes: onboard swing (roll), keel swing (pitch), and yaw. These are the standard designations used in the modeling of ships [5, 6]. In [5], the results of research as part of the improvement of the decision support system (DSS) were to formalize these designations in the design of ship power plants (SPP) for combined propulsion complexes (CPC). And in [6], the implemented DSS built by using system analysis, optimization, and modeling technologies aimed to implement this approach on the basis of *DMI*-models of ships. The issues of improving DSS by the method of mutual implementation of characteristic spatial vectors of energy processes in SPP and hydrodynamic in the CPC remained unresolved.

The announced method provides for a simple model the approximation of Coriolis terms and the damping matrix by a linear function. This system of equations of motion is based on [7] where the applied models require that the dynamics of the vessel and the ATs be known with a certain accuracy to use the linear-quadratic theory of optimal control. However, in this case, the identification of the mathematical model of the

vessel in a dynamic positioning mode (DP*)* is problematic since the excitation of the vessel under the action of DP is non-deterministic.

Different descriptions of excitation forces are based on [8] where models with four degrees of freedom are studied (where *roll* is an additional degree of freedom), and not with three, as in the case of [9] when the low-weight component is neglected. As for the three degrees of freedom, the equations are represented in the form of [10] where they are talking about controlling an autonomous underwater vehicle (*AUV*) with a linear-quadratic Gaussian controller and a combination of different algorithms. But the reported simulation results did not allow us to conclude that the fixed and variable speeds match. In [11], the problem of maneuvering is solved by parameterizing the input data on the basis of ensuring the desired dynamic behavior of the model. A technique of adaptive recursive design for a parametrically indefinite nonlinear object describing the dynamics of the vessel has been developed. First, the geometric part of the problem is solved. Then the law of renewal is built, which combines geometric design with a dynamic task. But the design procedure is carried out and tested by several experiments for the vessel model in the maritime control laboratory, which is not always possible.

On a classic marine vessel, drive forces originate from the rudder, fixed propellers, and thrusters (Ts). However, since the type of vessel in question is set in motion by the ATs, the reaction from the application of forces will be different. The ATs is an engine that can rotate 360 degrees around its vertical axis. This makes it possible to apply forces in the *x*- and *y*-directions depending on the position of the ATs and the torque applied to the vessel. Subsequent model calculations, which use input data from the speed of rotation, and azimuthal angle, were mainly obtained from model calculations [12]. The article analyzes parameter estimates for nonlinear regression models, where regressors are functions of a second-order module. The focus is on finding sequential estimates, and the instrumental variable method is used to this end. The problem of determining the accuracy of the appraiser remains unresolved if the input signal has a static displacement of sufficient amplitude, and the instruments are forced to have a non-zero average value of the time domain. These approaches were improved in [13] where more attention was paid to azimuthal forces as input data rather than rotational speeds. In [14] it is shown that this two-step procedure gives consistent estimates for second-order module models in cases where the standard applied method for finding sequential estimates does not work, in particular when measurement uncertainty is taken into account. In addition, it is shown that the possibility of obtaining consistent parameter estimates for models of this type depends on how the perturbations of the process enter the system, and on the volume of preliminary data on perturbation probability distributions that are available. In the cases where first-order moments are known, the aforementioned approach gives consistent estimates, even when perturbations enter the system before nonlinearity. To obtain consistent estimates in the cases where the moments of the first order are unknown, a structure is proposed to evaluate the moments of the first and second order along with the parameters of the model. This moment imposes additional requirements for the accuracy of measurement of these parameters.

To predict the states of the controller, it is necessary to use a monitoring system using sensors used in marine navigation. The main monitoring systems used in the control of the vessel are the inertial measurement unit (IMU) and the Global Positioning System (GPS).

IMU uses a combination of accelerometers, gyroscopes, and magnetometers to measure angular velocities, accelerations, and magnetic fields. It is an important device for controlling vessels as they can move and rotate in all 6 degrees of freedom. Measurements from the gyroscope and accelerometer include some shifts that create a systematic measurement error. If the angular velocities and accelerations are integrated, then as a result of linear velocity errors, they will increase linearly over time, and the orientation error – quadratically. Therefore, it will be difficult to rely only on IMU for this purpose over a longer period of time [15].

GPS is a system that uses satellite communication and data exchange with the receiver and providing information about location and time in areas with unhindered direct visibility. The most common GPS has For autonomous vehicles, the development and implementation of a high-integrity navigation system is based on the combined use of GPS and IMU. Improving the integrity of the navigation cycle will be carried out by identifying possible malfunctions both before and during the synthesis process. The implementation of this fault detection methodology takes into account both low-speed failures in IMU caused by displacement in sensor readings and device offset, as well as high-speed failures in the GPS receiver caused by multi-beam propagation errors.

The main purpose of the task of adequate vessel control is to minimize the design criterion, that is, to balance it between the magnitude of the tracking error $e=y–r$ and the value of the input signal. Sometimes such a paradigm can be considered as an optimization problem when a system is described using a linear differential equation, and integration relationships are described using quadratic functions.

To achieve the desired design behavior of the system, an iterative modeling and adjustment process is necessary in accordance with the behavior of the observed regulator in order to find the optimal value of constant coefficients. The controller defined above resets the state of the system to zero but, in this case, the controller must follow the specified reference signal.

A common problem that arises when modeling the yaw velocity is the unrealistic reaction of the model during the linearization of the input signal. When compared with a possible real reaction, almost any angle of α that is not close to the working value will differ significantly from the actual one. A possible solution for this problem is to use predictive amplification.

Predictive amplification is an approach to controlling a nonlinear system using multiple linear controllers. Thus, having several linearization species regarding the approximation of the trigonometric function at different operating points, LQR can be applied to these segments independently. A similar application of predictive LQR amplification, but in the field of risk management, was performed in [16], except for the problems of switching between linearization species [17]. If we neglect this aspect, then an unstable state or instability in the system may occur.

By using the Kalman filter to combine the information provided by the two sensors, it is possible to reduce the negative effects. The IMU offset can be adjusted, and when the GPS sensor is not in line of sight, the controller will rely more on IMU until the GPS reaches the line of sight again. However, since most maritime routes pass through areas with open skies, the GPS signal will always be present and therefore the focus will be on fixing the elimination of IMU. This type of integration of sensors for driving vehicles outdoors is implemented in [18] where ground transport is used instead of SBVs. In [19], the Kalman amplification coefficient is found using MATLAB/Simulink. First, an inertial system is developed to obtain information about the orientation and position of the control object. To determine the position and course, an algorithm for combining sensors using a standard Kalman filter is proposed. LQR methods and Kalman filtration are discussed in detail in [20]. Combined use of Kalman filtration and LQR is called linear-quadratic-gaussian control (LQG). Similar approaches to using such methods to solve such problems are considered in [21, 22]. In [21], a combination of equations describing the movement of a load by the mechanism for lifting the frame of the pallet holder into a system of differential equations with coefficients dependent on ship oscillations is proposed. In [22], the same approach is applied to the design of a linear-quadratic Gaussian regulator for a submarine. In both the first and second cases, the eigenvalues of a linear time-constant system can be optimally placed by modifying the performance criterion in the optimal controller design. The results are compared with the linear-quadratic Gauss controller, developed by standard methods of forming a cycle in the state assessment system and using a linear-quadratic regulator to restore cyclic transfer. The only thing that remains undefined is the method of assigning the eigenvalues of the optimal state feedback system.

Physical modeling begins with determining the SBVs coordinate system and how certain forces act on the SBVs in the aquatic environment. After that, it is explained how the thrusts and rotational moments of ATs affect SBVs depending on the angle and speed of rotation. These mathematical models are then combined to form a spatial vector of states in which the regulator will be applied. It then describes how LQR works and how to find the optimal controller using the Riccati model and equation [23]. It also explains how the following actions of the controller are activated, depending on possible changes in operating conditions. The results of a simulation research with the setting of the controller and controller of the reference input signals are analyzed in accordance with the achievement of the desired results. Also, during the simulation, the advantages of choosing different operating points for linearization of the model for different controller settings are investigated.

To take into account the existing restrictions, it will be necessary to adopt a number of simplifications. Some degrees of freedom (DOF) that have little effect on the system will be excluded. In modeling, we shall use only 3 degrees of freedom (DOF) out of 6 (pitching, roll, and yaw). Some parts of the resulting mathematical model will be nonlinear, so linearization will be necessary for the model to work with LQR. If it is impossible to obtain data from a real vessel, the modeling and design of the controller will be carried out using only nominal values.

3. The aim and objectives of the s research

The development of an optimal-parameter LCR for controlling SBVs with ATs in the aft part is reduced to a comparison, according to the results of modeling, of its work with actual conditions. This makes it possible to improve the control algorithms for scale models of SBVs based on the linear-quadratic principle of controlling thrusters.

To accomplish the aim, the following tasks have been set:

– to carry out physical modeling of SBVs with ATs in the aft part;

– to check the behavior of the model in combination with studies of the design features of vessels of this class;

– on the basis of the defined space of states and linearization of the AT control system, to simulate the yaw velocity to track the effect of disturbing forces on the characteristics of the controller;

– to determine the principles of linearization with independent control over the speed and angle of rotation of ATs;

– to define the limiting characteristics of azimuthal angles to adapt the controller to actual conditions.

4. Materials and research methods

4. 1. Methodology of iterative linearization of control system states

The position, orientation, and velocity of SBVs in accordance with the coordinate systems (Fig. 3) are based on hull symmetry around the X_bZ_b-plane, approximate symmetry around the Y_bZ_b-plane, and projection onto the Z_b-axis relative to the surface of the water. With this in mind, the position orientation vector and the linear-angular velocity vector can be defined as:

$$\bar{\varepsilon} \square [x \quad y \quad \varphi]^T, \; v \square [u \quad v \quad r]^T. \tag{1}$$

The usual simplification of the model is to neglect vertical movements (lifting/submerging) and longitudinal pitching ("pitching"). To simplify the model, the roll angle is also assumed to be small.

These generalized positions and velocities have a geometric relationship that can be described as

$$\varepsilon = J(\varepsilon)v, \tag{2}$$

and the equations of motion of the vessel in the inertial (fixed) coordinate system take the form

$$G_{MR}v + C_{MR}(v)v + D(v)v = \tau_{act}, \tag{3}$$

where G_{MR} is the inertia matrix of a solid, $C_{MR}(v)v$ represents centripetal and Coriolis terms, $D(v)$ is the damping matrix, τ_{act} is a vector with generalized external forces.

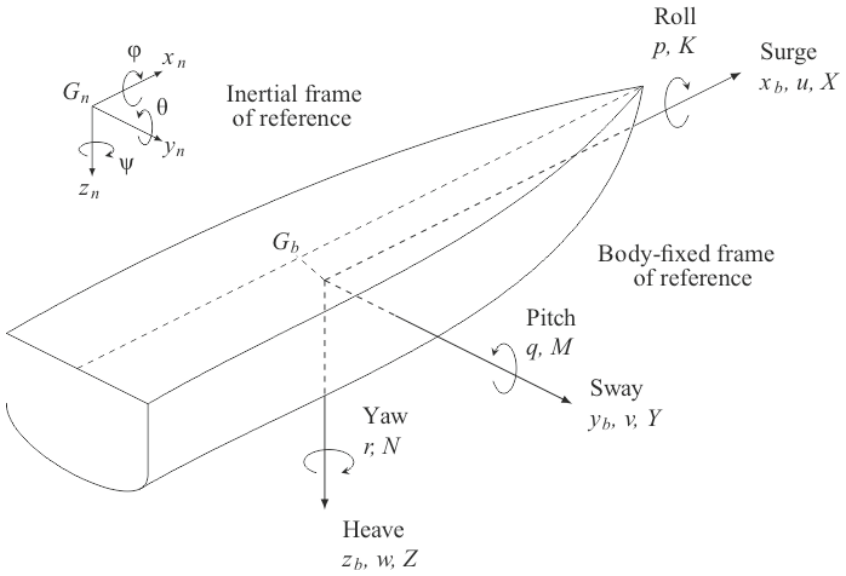

Fig. 3. Standard designations for describing the movement of a vessel in accordance with (1)

For three degrees of freedom, the equations are represented as follows:

$$J(\bar{\varepsilon})=\begin{bmatrix}\cos\varphi & -\sin\varphi & 0\\ \sin\varphi & \cos\varphi & 0\\ 0 & 0 & 1\end{bmatrix}, \tag{4}$$

$$G_{MR}=\begin{bmatrix} m & 0 & -y_G\\ 0 & m & mx_G\\ -my_G & mx_G & I_Z\end{bmatrix}, \tag{5}$$

$$C_{MR}(v)=\begin{bmatrix} 0 & -mr & -mx_Gr\\ mr & 0 & -my_Gr\\ mx_Gr & my_Gr & 0\end{bmatrix}, \tag{6}$$

$$D(v)=\begin{bmatrix} X_u & 0 & 0\\ 0 & Y_v & 0\\ 0 & 0 & N_r\end{bmatrix}, \tag{7}$$

where the total mass of the vessel is assumed to be equal to m and is found as $r_g=r_G=[x_G, y_G]$, as well as the I_z-inertia moment relative to the z-axis, expressed in the b-system. X_u, Y_v and N_r are large-scale damping coefficients.

Then the goal at this stage will be to find the law of control $u=-L_x$, where:

$$u=-Lx,\ \boldsymbol{L}=\arg\min_{L}\int_0^{\infty}\left(z^T(t)Q_1z(t)+u^T(t)Q_2u(t)\right)\mathrm{d}t, \tag{8}$$

where Q_1 and Q_2 are weight matrices that can be used as design variables for the resulting controller. The solution of the optimization problem is carried out by determining:

$$L=Q_2^{-1}B^TS^N, \tag{9}$$

where S^N is a positively defined matrix that solves the Riccati algebra equation:

$$A^T S^N + S^N A + M^2 Q_1 M - S^N B Q_2^{-1} B^T S^N = 0. \quad (10)$$

The solution to this equation can be derived using MATLAB Simulink software. To do this, you need to integrate the reference signal *ref* in the equations:

$$u(t) = -Lx(t) + L_{ref} ref\,(t), \quad (11)$$

where L_{ref} is selected so that the static gain corresponds to a given value. A similar method of using LQR was applied in [24]. The system developed according to this principle is shown in Fig. 4.

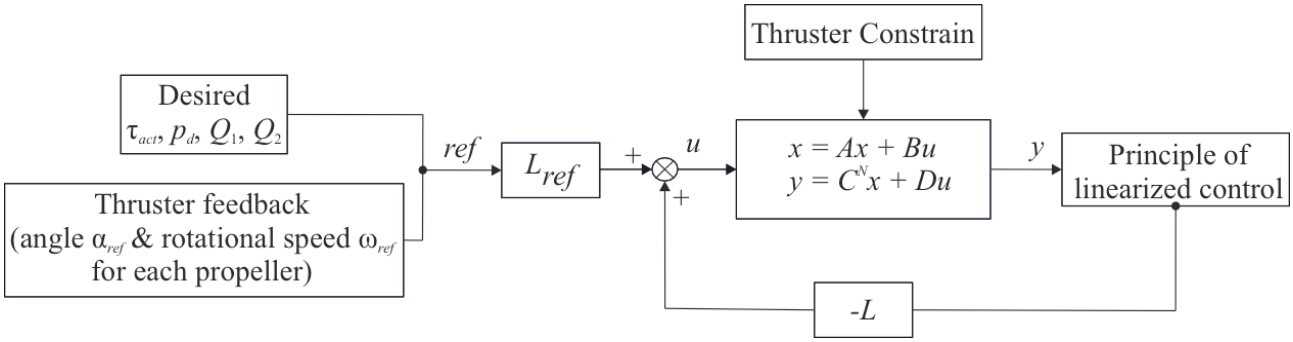

Fig. 4. Designation of the reference signal and system feedback

Each system is characterized by uncertainties. Typically, these uncertainties are modeled as a random stochastic process ("white noise"), which is a random signal with a constant spectrum. Given the uncertainty, the model can be written as

$$\dot{x} = Ax + Bu + Nv_1, \; \cdot = C^N x + v_2, \; \dot{z} = G_{MR} x, \quad (12)$$

where v_1 and v_2 are white "Gaussian" noise with normal distribution in the time region with zero mean value of the time region. In order to filter out these signals, a state observer can be implemented that uses the estimate in the following form:

$$\hat{x} = A\hat{x} = Bu + K\left(y - C^N \hat{x}\right) = \left(A - KC^N\right)\hat{x} + Bu + Ky. \quad (13)$$

This problem can be solved by describing it as an optimization problem by analogy with the definition of LQR with minimizing the variance of the valuation error. If the system error is designated as $e = x - \hat{x},$ then the variance will be equal to $E_e(t)e(t)$. If v_1 and v_2 are independent and have a normal distribution in the time domain with a zero mean value of the time domain, we can assume that:

$$E_e v_1 v_1^T = V_1, \; E_e v_2 v_2^T = V_2, \; E_e v_1 v_2^T = 0. \quad (14)$$

Then the state observer can be described as

$$K = \operatorname{cov} PC^{N} V_2^{-1}, \tag{15}$$

where cov$P$ is the covariation matrix of the optimal estimate that solves the Riccati equation

$$A^T \operatorname{cov} P + \operatorname{cov} PA + N_\alpha V_1 N_\alpha^T - \\ -\operatorname{cov} PC^T V_2^{-1} C^{N_\alpha} \operatorname{cov} P = 0. \tag{16}$$

(16) is called a Kalman filter, where V_1 and V_2 are variables that can be configured to filter process perturbation and measurement.

Suppose that the force N_α of ATs is applied to the hull of the vessel. Let the thruster be the AT that rotates at the speed of rotation of the propeller ω_i (r/s), and the angle of the applied resulting force α_i (rad). Then the forces in the x_b-direction from the azimuthal motor i can be designated as (Fig. 5):

$$F_{x,i} = g_x\left(\omega_i, \alpha_i, u_{\alpha,i}\right), \tag{17}$$

where $u_{\alpha,i}$ is the velocity of water passing through ATs in the negative direction x_b. This is necessary because at higher speeds, and when $u_{\alpha,i}$ and $\omega_i \cos(\alpha_i)$ are equal to the same sign, there will be a loss of efficiency. The assumption in the model is a linear relationship between g_x and ω_i as

$$g_x\left(\omega_i, \alpha_i, u_{\alpha,i}\right) = \mu_i \omega_i \cos(\alpha_i) - k_i \omega_i u_{\alpha,i} \cos(\alpha_i), \tag{18}$$

where μ_i and k_i are positive constants defined by a full-scale experiment, and $u_{\alpha,\mathrm{i}}$ can be described as

$$u_{\alpha,i} = (1 - w_i) u_r. \tag{19}$$

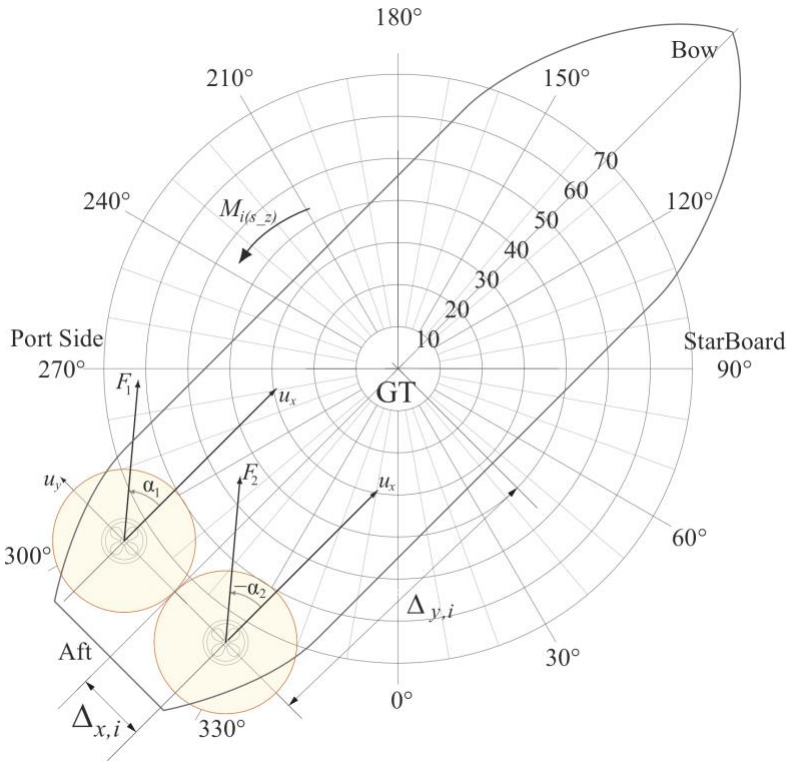

Fig. 5. Location and angle of rotation of the *i*-th AT

Here, w_i is the coefficient of the passing flow, which determines the ratio of the speed of water flowing through the propeller to the speed of the vessel u_r – the relative speed between the vessel and the surrounding water. By combining the coefficient of passing flow, we can simplify the second term in (18) using

$$k_i = (1 - w_i) k_i', \tag{20}$$

and substituting this in (18), we get

$$g_x(\omega_i, \alpha_i, u_r) = \mu_i \omega_i \cos(\alpha_i) - k_i \omega_i u_r \cos(\alpha_i). \tag{21}$$

Thus, we have a generalized model of forces from ATs. However, the true function $g_x(\cdot)$ is more complex due to water dynamics but the approximate function would be adequate for the purposes of this research.

Similarly, the force in the Y_b-direction

$$\begin{aligned} F_{y,i} &= g_y(\omega_i, \alpha_i, v_r) = \mu_i \omega_i \sin(\alpha_i) - k_i' \omega_i v_{a,i} \sin(\alpha_i) = \\ &= \mu_i \omega_i \sin(\alpha_i) - k_i \omega_i u_r \sin(\alpha_i), \end{aligned} \tag{22}$$

can be found with the same assumptions as for the *x*-direction. The azimuthal engine *i* will also generate torque relative to the vessel depending on where it is installed relative to the center of rotation of the vessel. Torque can be described as

$$M_i = \Delta_{x,i} F_{y,i} - \Delta_{y,i} F_{x,i}. \tag{23}$$

The generalized torque vector contains forces and moments from all azimuthal motors put together.

$$\tau_{act} = \begin{bmatrix} \sum_{i=1}^{N_\alpha} \mu_i \omega_i \cos(\alpha_i) - k_i \omega_i u_r \cos(\alpha_i) \\ \sum_{i=1}^{N_\alpha} \mu_i \omega_i \sin(\alpha_i) - k_i \omega_i u_r \sin(\alpha_i) \\ \sum_{i=1}^{N_\alpha} \omega_i \begin{bmatrix} \mu_i \left(\Delta_{x,i} \sin(\alpha_i) - \Delta_{y,i} \cos(\alpha_i) \right) - \\ -k_i \left(\Delta_{x,i} v_r \sin(\alpha_i) - \Delta_{y,i} u_r \cos(\alpha_i) \right) \end{bmatrix} \end{bmatrix}, \tag{24}$$

To make the model even easier, we neglect the losses at high speed in the y_b direction since the speeds in this direction are much lower than in the x_b direction.

Also, for simplicity, it is assumed that each engine is equally efficient and therefore

$$\mu_i = \mu_j \; \mu \forall i, j = 1, \ldots, N_\alpha, \; k_i = k_j \; -k \forall i, j = 1, \ldots, N_\alpha. \tag{25}$$

which yields

$$\tau_{act} = \begin{bmatrix} \sum_{i=1}^{N_\alpha} \mu \omega_i \cos(\alpha_i) + k \omega_i u_r \cos(\alpha_i) \\ \sum_{i=1}^{N_\alpha} \mu \omega_i \sin(\alpha_i) \\ \sum_{i=1}^{N_\alpha} \mu \omega_i \left(\Delta_{x,i} \sin(\alpha_i) - \Delta_{y,i} \cos(\alpha_i)(1 - k u_r) \right) \end{bmatrix}. \tag{26}$$

Since τ_{act} depends on u_r, which, in turn, depends on the rate of increase in motion resistance, the model becomes nonlinear. For simplicity, we neglect these terms and the designation of a generalized torque vector can be simplified to

$$\tau_{act} = \begin{bmatrix} \mu \tilde{\tau}_x \\ \mu \tilde{\tau}_y \\ \mu \tilde{\tau}_\varphi \end{bmatrix} = \begin{bmatrix} \mu \sum_{i=1}^{N_\alpha} \omega_i \cos(\alpha_i) \\ \mu \sum_{i=1}^{N_\alpha} \omega_i \sin(\alpha_i) \\ \mu \sum_{i=1}^{N_\alpha} \omega_i \left(\Delta_{x,i} \sin(\alpha_i) - \Delta_{y,i} \cos(\alpha_i) \right) \end{bmatrix}. \tag{27}$$

Since $C_{MR}(\nu)$ depends on ν, the term $C_{MR}(\nu)\nu$ becomes nonlinear. However, the use of LQR requires a linear model. Thus, linearization is needed to simplify the model further. Linearization is described by the function

$$L(x) = f(a) + f'(a)(x - a), \tag{28}$$

where $L(x)$ is called a linearized function, $f(\alpha)$ is a function to be linearized in α, $f'(\alpha)$ is a derivative of $f(x)$ over x, estimated in (α), in this case the Jacobian of function $f(\mathbf{x})$.

Finally, x – linearization variable (in this case, ν), α is the selected operating point (angle of rotation of AT relative to the body of SBV. In this case, the linearizing terms are equal to:

$$f(v)=C_{MR}(v)v= \\ =\begin{bmatrix} 0 & -mr & -mx_{G_{MR}}r \\ mr & 0 & -my_{G_{MR}}r \\ mx_{G_{MR}}r & my_{G_{MR}}r & 0 \end{bmatrix}\begin{bmatrix} y \\ v \\ r \end{bmatrix}= \\ =\begin{bmatrix} -mrv-mx_{G_{MR}}r^2 \\ mrv-my_{G_{MR}}r^2 \\ mx_{G_{MR}}ru+my_{G_{MR}}rv \end{bmatrix}, \tag{29}$$

which contains Jacobian

$$J(v)=\begin{bmatrix} 0 & -mr & -mr & -2mx_{G_{MR}}r \\ mr & 0 & mu & -2my_{G_{MR}}r \\ mx_{G_{MR}}r & my_{G_{MR}}r & mx_{G_{MR}}u & +my_{G_{MR}}v \end{bmatrix}. \tag{30}$$

The operating point depends on what state the system should be. Since the system will operate at a constant forward speed and with minor changes in the speed of rotation of AT, the corresponding operating point is defined as

$$a=\begin{bmatrix} u_0 \\ v_0 \\ r_0 \end{bmatrix}=\begin{bmatrix} 1 \\ 0 \\ 0 \end{bmatrix}. \tag{31}$$

Using this working point and linearizing $C_{RB}(\nu)\nu$, we find the following

$$L(v)=\begin{bmatrix} 0 & 0 & 0 \\ 0 & 0 & m \\ 0 & 0 & mx_{G_{MR}} \end{bmatrix}\begin{bmatrix} u \\ v \\ r \end{bmatrix}. \tag{32}$$

The matrix of states (32) will then replace $C_{MR}(\nu)\nu$ in the equation of the space of states.

4. 2. Linearization of the assigned input signal

To control a vessel using an AT, it is necessary to process drive signals as input signals, so the complete equation (26) must be combined into a controller with a dependence on ω and α. Due to the trigonometric functions of cos and sin, which are present in (27), linearization with the LQR framework is necessary to match it.

Linearization of the general case is as follows. Since there are several operating points that can be selected in the simulation, a general case of linearization is necessary. In addition, two different linearization species are needed through two ways to control the vessel. One with synchronous control, that is, the same input signals for both ATs,

and one with differential (asynchronous) control, where the Ats are controlled independently. Starting with synchronous control, we use the following variables

$$\operatorname{cov} P_s = \begin{bmatrix} \omega_i \\ \alpha_i \end{bmatrix}. \tag{33}$$

Then (28) integrates to (27) with the previously mentioned variable and the generalized working point as α_s

$$f(p) = \tau(p) = \begin{bmatrix} \sum_{i=1}^{N_\alpha} \omega_i \cos(\alpha_i) \\ \sum_{i=1}^{N_\alpha} \omega_i \sin(\alpha_i) \\ \sum_{i=1}^{N_\alpha} \omega_i \left(\Delta_{x,i} \sin(\alpha_i) - \Delta_{y,i} \cos(\alpha_i) \right) \end{bmatrix}, \tag{34}$$

$$J(p) = \\ = \sum_{i=1}^{N_\alpha} \begin{bmatrix} \cos(\alpha_i) & -n_i \sin(\alpha_i) \\ \sin(\alpha_i) & n_i \cos(\alpha_i) \\ \left(\Delta_{x,i} \sin(\alpha_i) - \Delta_{y,i} \cos(\alpha_i) \right) & \left(\Delta_{x,i} \sin(\alpha_i) + \Delta_{y,i} \cos(\alpha_i) \right) \end{bmatrix},$$

$$a_s = \begin{bmatrix} \bar{\omega} \\ \bar{\alpha} \end{bmatrix}, \tag{35}$$

which gives the following equation, which includes a constant term:

$$L(p) = \sum_{i=1}^{N_\alpha} \begin{bmatrix} \bar{\omega} \cos\bar{\alpha} \\ \bar{\omega} \sin\bar{\alpha} \\ \bar{\omega} \left(\Delta_{x,i} \sin\bar{\alpha} - \Delta_{y,i} \cos\bar{\alpha} \right) \end{bmatrix} + \\ + \sum_{i=1}^{N_\alpha} \begin{bmatrix} \cos\bar{\alpha} & -\bar{\omega} \sin\bar{\alpha} \\ \sin\bar{\alpha} & \bar{\omega} \cos\bar{\alpha} \\ \left(\Delta_{x,i} \sin\bar{\alpha} - \Delta_{y,i} \cos\bar{\alpha} \right) & \left(\Delta_{x,i} \sin\bar{\alpha} + \Delta_{y,i} \cos\bar{\alpha} \right) \end{bmatrix} \begin{bmatrix} y'\omega \\ \bar{\alpha} \end{bmatrix}. \tag{36}$$

This means that the stable state of ATs must be at this operating point and the controller will control deviations from this state. In other words, τ_{act} can be divided into two parts as follows:

$$\tau_{act} = \bar{\tau}_{act} + \tilde{\tau}_{act}, \tag{37}$$

where $\bar{\tau}_{act}$ is constant, and:

$$\tilde{\tau}_{act} = \\ = \sum_{i=1}^{N_\alpha} \begin{bmatrix} \cos\bar{\alpha} & -\bar{\omega}\sin\bar{\alpha} \\ \sin\bar{\alpha} & \bar{\omega}\cos\bar{\alpha} \\ \Delta_{x,i}\sin\bar{\alpha} - \Delta_{y,i}\cos\bar{\alpha} & \Delta_{x,i}\sin\bar{\alpha} + \Delta_{y,i}\cos\bar{\alpha} \end{bmatrix} \begin{bmatrix} \omega \\ \alpha \end{bmatrix}, \tag{38}$$

depends on the time that will be determined by the LQ controller. This linearization will force the ATs to use the same rotational speed and propeller flow angle for both ATs.

For differential (asynchronous) control, the control variable will contain a separate definition of the control signal:

$$p_d = \begin{bmatrix} \omega_1 & \omega_2 & \alpha_1 & \alpha_2 \end{bmatrix}^T. \tag{39}$$

where the speed of rotation of the propeller and the angle of the applied resulting force, respectively: ω_1, α_1 – port side, ω_2, α_2 – starboard.

As before, equation (28) is applied and a new Jacobi matrix is displayed and a working point is used. However, for $f(p_d)$ is still chosen (34) since these equations must also undergo a linearization procedure. The reworked equations are as follows:

$$J(p_d) = \\ = \begin{bmatrix} \cos\alpha_1 & \sin\alpha_1 & \Delta_{x1}\sin\alpha_1 - \Delta_{y1}\cos\alpha_1 \\ \cos\alpha_2 & \sin\alpha_2 & \Delta_{x,2}\sin\alpha_2 - \Delta_{y,2}\cos\alpha_2 \\ -\omega_1\sin\alpha_1 & \omega_1\cos\alpha_1 & \omega_1\left(\Delta_{x1}\cos\alpha_1 + \Delta_{y1}\sin\alpha_1\right) \\ \omega_2\sin\alpha_2 & \omega_2\cos\alpha_2 & \omega_2\left(\Delta_{x,2}\cos\alpha_2 + \Delta_{y,2}\sin\alpha_2\right) \end{bmatrix}^T,$$

$$a_d = \begin{bmatrix} \bar{\omega}_1 & \bar{\omega}_2 & \bar{\alpha}_1 & \bar{\alpha}_2 \end{bmatrix}^T. \tag{40}$$

These transformations give complete linearization:

$$L(\rho_d) = \begin{bmatrix} \bar{\omega}_1\cos\bar{\alpha}_1 + \bar{\omega}_2\cos\bar{\alpha}_2 \\ \bar{\omega}_1\sin\bar{\alpha}_1 + \bar{\omega}_2\sin\bar{\alpha}_2 \\ \bar{\omega}_1\left(\Delta_{x1}\sin\bar{\alpha}_1 - \Delta_{y1}\cos\bar{\alpha}_1\right) + \bar{\omega}_2\left(\Delta_{x,2}\sin\bar{\alpha}_2 - \Delta_{y,2}\cos\bar{\alpha}_2\right) \end{bmatrix} + \\ + \begin{bmatrix} \cos\bar{\alpha}_1 & \sin\bar{\alpha}_1 & \Delta_{x1}\sin\bar{\alpha}_1 - \Delta_{y1}\cos\bar{\alpha}_1 \\ \cos\bar{\alpha}_2 & \sin\bar{\alpha}_2 & \Delta_{x,2}\sin\bar{\alpha}_2 - \Delta_{y,2}\cos\bar{\alpha}_2 \\ -\bar{\omega}_1\sin\bar{\alpha}_1 & \bar{\omega}_1\cos\bar{\alpha}_1 & \bar{\omega}_1\left(\Delta_{x1}\sin\bar{\alpha}_1 + \Delta_{y1}\cos\bar{\alpha}_1\right) \\ -\bar{\omega}_2\sin\bar{\alpha}_2 & \bar{\omega}_2\cos\bar{\alpha}_2 & \bar{\omega}_2\left(\Delta_{x,2}\sin\bar{\alpha}_2 + \Delta_{y,2}\cos\bar{\alpha}_2\right) \end{bmatrix}^T \begin{bmatrix} \omega_1 \\ \omega_2 \\ \alpha_1 \\ \alpha_2 \end{bmatrix}. \tag{41}$$

and differential (asynchronous) control signal:

$$\tilde{\tau}_{act} = \begin{bmatrix} \cos\bar{\alpha}_1 & \sin\bar{\alpha}_1 & \Delta_{x1}\sin\bar{\alpha}_1 - \Delta_{y1}\cos\bar{\alpha}_1 \\ \cos\bar{\alpha}_2 & \sin\bar{\alpha}_2 & \Delta_{x,2}\sin\bar{\alpha}_2 - \Delta_{y,2}\cos\bar{\alpha}_2 \\ -\bar{\omega}_1\sin\bar{\alpha}_1 & \bar{\omega}_1\cos\bar{\alpha}_1 & \bar{\omega}_1\left(\Delta_{x1}\sin\bar{\alpha}_1 + \Delta_{y1}\cos\bar{\alpha}_1\right) \\ -\bar{\omega}_2\sin\bar{\alpha}_2 & \bar{\omega}_2\cos\bar{\alpha}_2 & \bar{\omega}_2\left(\Delta_{x,2}\sin\bar{\alpha}_2 + \Delta_{y,2}\cos\bar{\alpha}_2\right) \end{bmatrix}^T \begin{bmatrix} \omega_1 \\ \omega_2 \\ \alpha_1 \\ \alpha_2 \end{bmatrix}. \tag{42}$$

With the help of such linearization, it is possible to describe the functions of an independent change in the speed of rotation and the angles of location of AT engines.

4. 3. Determination of a coherent position with linearization function

For a simplified model, some position points give the best results depending on the expected maneuver of the vehicle. The simplified trigonometric orientation function of the AT motor is an important aspect when a position determination point is selected because they are periodic. After linearization, the trigonometric function loses its characteristic behavior, and a higher value always leads to an increase in torque. Therefore, the obtained simulation results must correspond to the point of determining the position *i* in order to have the result closest to reality. For the rotating scenario of the model, a nonzero value of α for the selected algorithm would be reasonable, and for a sharp change in the trajectory, a higher value of ω and a zero value of α. These two different approaches will be used for linearization and they are described as follows, starting with an algorithm for abruptly changing the ship's trajectory (an increasing algorithm):

$$\alpha = \begin{bmatrix} 20 \\ 0 \end{bmatrix}. \tag{43}$$

Using this point of determining the position, which is determined by the optimal angle of α, and substituting the values Δx_i and Δy_i for both ATs in (38), we get

$$\tilde{\tau}_{act} = \begin{bmatrix} 4 & 0 \\ 0 & 52 \\ 0 & -22 \end{bmatrix} \begin{bmatrix} \omega \\ \alpha \end{bmatrix}. \tag{44}$$

For the ship's turning algorithm, the position determination point is determined as follows:

$$\alpha = \begin{bmatrix} 10 \\ -\pi / 6 \end{bmatrix}, \tag{45}$$

adjusted to match the nonzero angle of AT propellers. The turning speed also decreased. By inserting these value $\Delta_{x,i}$ and $\Delta_{y,i}$ in (38), we get:

$$\tilde{\tau}_{act} = \begin{bmatrix} \sqrt{3} & 10 \\ -1 & 10\sqrt{3} \\ 0.6 & -4\sqrt{3} \end{bmatrix} \begin{bmatrix} \omega \\ \alpha \end{bmatrix}. \tag{46}$$

These will be two different linearization species that will be used in the simulation. Theoretically, the latter should give better results when modeling with an increased yaw velocity. We get two points for determining the position:

$$a_d = [26 \quad 26 \quad 0 \quad 0]^T,$$

$$a_d = \begin{bmatrix} 12 & 12 & -\pi/6 & -\pi/6 \end{bmatrix}^T, \qquad (47)$$

which will also be used for differential linearization and have equivalent values. These points of position determination define the following equations:

$$\tilde{\tau}_{act} = \begin{bmatrix} 1 & 1 & 0 & 0 \\ 0 & 0 & 26 & 26 \\ -0.2 & 0.2 & -12 & -12 \end{bmatrix} \times \begin{bmatrix} \omega_1 \\ \omega_2 \\ \alpha_1 \\ \alpha_2 \end{bmatrix},$$

$$\tilde{\tau}_{act} = \begin{bmatrix} \frac{\sqrt{3}}{2} & \frac{\sqrt{3}}{2} & 7 & 7 \\ -\frac{1}{2} & -\frac{1}{2} & 7\sqrt{3} & 7\sqrt{3} \\ \frac{6-\sqrt{3}}{26} & \frac{\sqrt{3}+6}{26} & -\frac{1+6\sqrt{3}}{2} & \frac{1-6\sqrt{3}}{2} \end{bmatrix} \times \begin{bmatrix} \omega_1 \\ \omega_2 \\ \alpha_1 \\ \alpha_2 \end{bmatrix}. \qquad (48)$$

Such linearization can increase the maneuverability of the vessel and create different approaches to solving the control problem.

4. 4. Definition of the space of states

To use LQR, the model must be defined in the form of a space of states:

$$\dot{x} = \boldsymbol{A}x + \boldsymbol{B}u, \; y = \boldsymbol{C}_N x + \boldsymbol{D}u, \qquad (49)$$

where x – controlled states, u – input signals, y – output signals, A – state matrix, B – input matrix, C_N – output matrix, and D – direct bond matrix. So the inverse matrix G_{MR} (3) must be written as:

$$\dot{v} = G_{MR}^{-1}\left(-L(v) - D(v)v + \tau_{act}\right). \qquad (50)$$

Using this equation and substituting parameters and variables from (5), (7), and (32), it is possible to simplify the equation for τ_{act}. τ_{act} will be replaced by $\tilde{\tau}_{act}$, which is one of the linearized parameters. The equation can be simplified as follows:

$$\dot{v}=\begin{bmatrix}\dot{u}\\ \dot{v}\\ \dot{r}\end{bmatrix}=$$

$$=\begin{bmatrix}\frac{mx_{G_{MR}}^2-I_z}{m^2x_{G_{MR}}^2+m^2y_{G_{MR}}^2-I_zm} & \frac{x_{G_{MR}}y_{G_{MR}}}{m^2x_{G_{MR}}^2+m^2y_{G_{MR}}^2-I_Z} & \frac{-y_{G_{MR}}}{m^2x_{G_{MR}}^2+m^2y_{G_{MR}}^2-I_Z}\\ \frac{x_{G_{MR}}y_{G_{MR}}}{mx_{G_{MR}}^2+my_{G_{MR}}^2-I_Z} & \frac{my_{G_{MR}}^2-I_Z}{m^2x_{G_{MR}}^2+m^2y_{G_{MR}}^2-I_Z} & \frac{x_G}{mx_{G_{MR}}^2+my_{G_{MR}}^2-I_Z}\\ \frac{-y_{G_{MR}}}{mx_{G_{MR}}^2+my_{G_{MR}}^2-I_Z} & \frac{x_{G_{MR}}}{mx_{G_{MR}}^2+my_{G_{MR}}^2-I_Z} & \frac{-1}{mx_{G_{MR}}^2+my_{G_{MR}}^2-I_Z}\end{bmatrix}\times$$

$$\times\left(-\begin{bmatrix}0&0&0\\0&0&m\\0&0&mx_{G_{MR}}\end{bmatrix}\begin{bmatrix}u\\v\\r\end{bmatrix}-\begin{bmatrix}X_uu&0&0\\0&Y_vv&0\\0&0&N_rr\end{bmatrix}+\mu\tilde{\tau}_{act}\right)=$$

$$=\left(\frac{1}{mx_{G_{MR}}^2+my_{G_{MR}}^2-I_Z}\right)\left(\begin{bmatrix}\frac{mx_{G_{MR}}^2-I_z}{m} & x_{G_{MR}}y_{G_{MR}} & -y_{G_{MR}}\\ x_{G_{MR}}y_{G_{MR}} & \frac{my_{G_{MR}}^2-I_Z}{m} & x_{G_{MR}}\\ -y_{G_{MR}} & x_{G_{MR}} & -1\end{bmatrix}\right)\mu\tilde{\tau}_{act}-$$

$$-\begin{bmatrix}\frac{x_u\left(mx_{G_{MR}}^2-I_z\right)}{m} & Y_vx_{G_{MR}}y_{G_{MR}} & -N_ry_{G_{MR}}\\ X_ux_{G_{MR}}y_{G_{MR}} & Y_v\left(mx_{G_{MR}}^2-I_z\right) & N_rx_{G_{MR}}-mx_{G_{MR}}^2-my_{G_{MR}}^2+I_z\\ -X_uy_{G_{MR}} & Y_vx_{G_{MR}} & -N_r\end{bmatrix}\begin{bmatrix}u\\v\\r\end{bmatrix}. \quad (51)$$

Assuming that the value $\bar{r}_{G_{MR}}$ is significantly small, it can be brought closer to 0. Then the equation for *v* can be simplified even more:

$$\dot{v}=\begin{bmatrix}-\frac{X_u}{m}&0&0\\0&-\frac{Y_u}{m}&1\\0&0&-\frac{N_r}{I_z}\end{bmatrix}\times\begin{bmatrix}u\\v\\r\end{bmatrix}+$$

$$+\begin{bmatrix}-\frac{\mu}{m}&0&0\\0&-\frac{\mu}{m}&0\\0&0&-\frac{\mu}{I_z}\end{bmatrix}\tilde{\tau}_{act}. \quad (52)$$

The resulting form can be considered as a representation of the space of states, where:

$$x=v,\ u=\begin{bmatrix}\omega\\ \alpha\end{bmatrix},\ A=\begin{bmatrix}-\frac{X_u}{m}&0&0\\0&-\frac{Y_v}{m}&1\\0&0&-\frac{N_r}{I_z}\end{bmatrix},$$

$$B=\begin{bmatrix} -\frac{\mu}{m} & 0 & 0 \\ 0 & -\frac{\mu}{m} & 0 \\ 0 & 0 & -\frac{\mu}{I_z} \end{bmatrix}\tilde{\tau}_{act}. \qquad (53)$$

The sensors used to determine the speed and position of the vessel are in a moving coordinate system, which leads to the following definitions:

$$y=\begin{bmatrix} u \\ v \\ r \end{bmatrix}, C_N=\begin{bmatrix} 1 & 0 & 0 \\ 0 & 1 & 0 \\ 0 & 0 & 1 \end{bmatrix}, D=\begin{bmatrix} 0 & 0 \\ 0 & 0 \\ 0 & 0 \end{bmatrix}. \qquad (54)$$

B will vary depending on the linearization of the input signal used, for example if (44) and (46) are used. From (2) and (4) these values can be transferred to the ω-system, where it is assumed that ψ=0.

5. The results of researching the method of linear-quadratic control over the physical model of ta vessel with azimuthal thrusters

5. 1. Physical modeling of elements for a sea-based vehicle

The physical scale model of SBVs is based on a controller that uses input data from GPS and IMU to determine the position, course, and speed of the vessel. Based on these data, the controller will control the actuators, an electronically commutated motor (ECM), and a servo drive for each AT. ECM is connected to the AT propeller through gear transmissions (Fig. 6). The gear ratio between the servo drive and the AT compound is quite large. The main characteristics of the formalized physical model of AT are shown in Fig. 7.

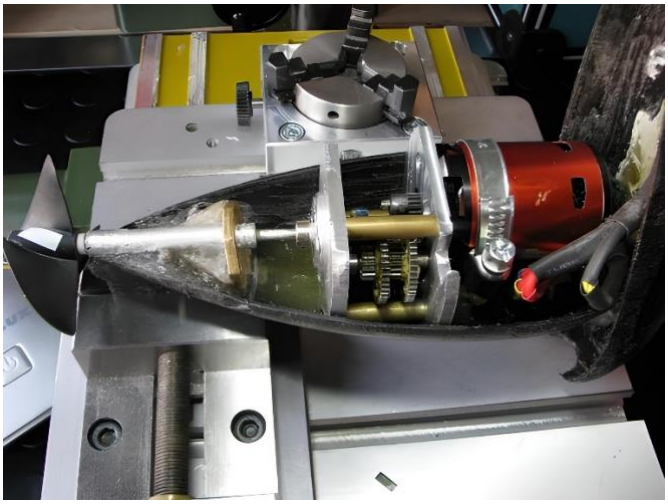

Fig. 6. Gear transmission connecting the electronically commutated motor with the propeller of the azimuthal thruster

To regulate the rotational speed and torque of ECM, the motor currents are measured and the throughput is calculated with high accuracy (Fig. 6). Torque control is an integral part of the design of most applied speed control circuits of AT electric drive systems. Theoretically, the time of increase in the torque in the frequency converter (FC) with pulsed width modulation (PWM) is limited by the inductance of the motor in dependent current inverters with a DC link [25]. However, in practice, the controller limits the rate of change in torque to prevent damage to the mechanical part of the electric drive.

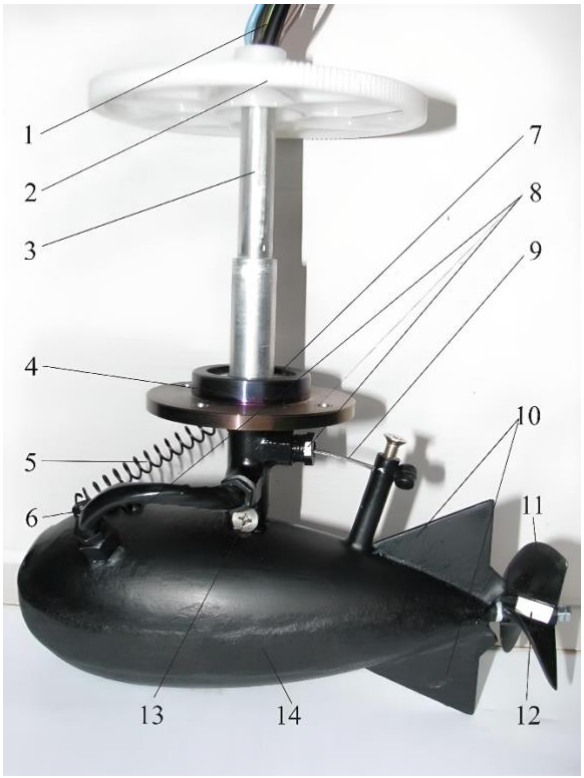

Fig. 7. Physical model of the thruster with two degrees of freedom: 1 – electronically commutated motor supply cable and a drive cable for changing the angle of inclination; 2 – drive gear of the baller's turn drive; 3 – baller; 4 – bearing shield; 5 – feedback spring of the drive for changing the angle of inclination; 6 – supply cable; 7 – support bearing; 8 – oil seal inputs; 9 – rope of the drive for changing the angle of inclination; 10 – stabilization wings; 11 – fixed pitch propeller; 12 – fluorescent mark for remote measurement of the rotational speed of the fixed pitch propeller; 13 – the place of connection of the baller with the body of the azimuthal thruster; 14 – body of an azimuthal thruster with an electronically commutated motor located inside

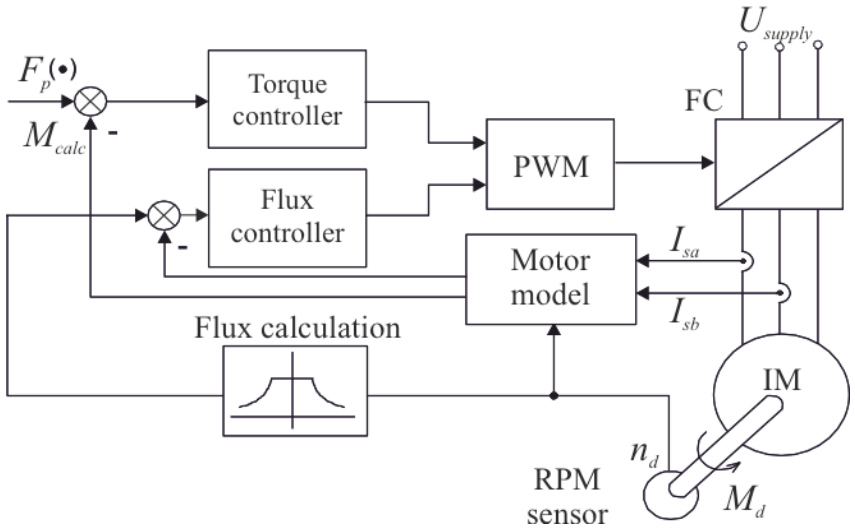

Fig. 8. Block diagram of a closed system for controlling the torque of an electronically commutated motor of the azimuthal thruster: Ψ_p and Ψ_{calc} – values of the assigned and calculated flows, I_{sa}, I_{sb} – measured values of stator currents; PWM – pulse-width modulation; IM – induction motor; FC – frequency convertor

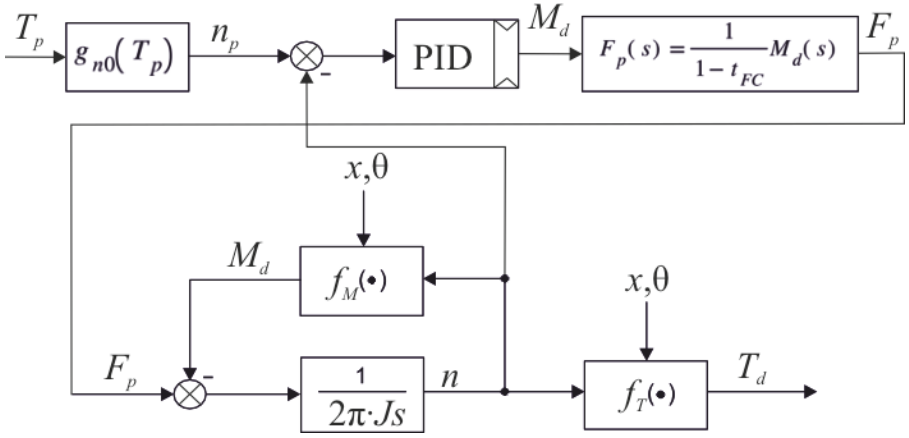

Fig. 9. Block diagram of the speed controller in an electronically commutated motor

Thus, the transfer function of the controller can be described by dependence

$$F_p(s) = \frac{1}{1-t_{\text{п ч}}} M_d(s), \qquad (55)$$

where t_{FC}=20…200 ms.

5. 2. Checking the behavior of SBV model when modeling surge

To check the behavior of the model and determine whether the controller can control the system, a simulation research is carried out to check certain properties of the system. Each simulation is performed with simultaneous and differential control of ATs [26–34].

For GFC, the interaction between the torque of the propeller M_p, which is determined by the push force F_p, the thrust T_p and the power P_p of the propeller, is found on the basis of the diagram of free water and the dynamics equations regarding the shaft speed and the diameter of the propeller [35]:

$$\left.\begin{aligned} T_p &= \rho D_p^4 \cdot K_T \cdot \omega \cdot |\omega|; \\ M_p &= \rho D_p^5 \cdot K_F \cdot \omega \cdot |\omega|; \\ P_p &= 2\pi\omega \cdot M_p, \end{aligned}\right\} \quad (56)$$

where ω – propeller speed, r/s; ρ – density of water, kg/m^3; D_p – propeller diameter, m; K_T – propeller thrust factor; K_F is the coefficient of momentum.

The relative pitch of the propeller λ (H_p)=υ_a/(ωD_p), where υ_a is the speed of water inflow to the propeller. The efficiency of using the propeller in open water is defined as the ratio of the work performed by the propeller to obtain the thrust force to work necessary to overcome the torque on the shaft:

$$\eta_b = \frac{\upsilon_a \cdot M_p}{2\pi\omega T_p} = \frac{\lambda}{2\pi} \cdot \frac{K_T}{K_F}. \quad (57)$$

As an initial test, a simple speed jump was made. This is done both for synchronous steering, when the input signals for both ATs are the same, and for differential (asynchronous), when the ATs can be controlled independently. Both simulations are performed using the linearization of the drive, where α is zero (46).

5. 2. 1. Synchronous control over aft azimuthal thrusters

The purpose of setting was to get a relatively fast transient characteristic with minimal overshooting, so the emphasis was on minimizing tracking errors. This is mainly done in order to see the relationship between the speed of rotation of the propellers and the characteristics of the load surge, as well as how the angle of the propeller, close to zero, behaves. Weight matrices and reference gain will be determined as follows:

$$Q_1 = \begin{bmatrix} 120 & 0 & 0 \\ 0 & 1 & 0 \\ 0 & 0 & 1 \end{bmatrix}, \quad Q_2 = \begin{bmatrix} 1 & 0 \\ 0 & 1 \end{bmatrix}, \quad Q_3 = \begin{bmatrix} 10 & 0 & 0 \\ 0 & 0 & 0 \end{bmatrix}, \quad (58)$$

giving the results shown in Fig. 10–12.

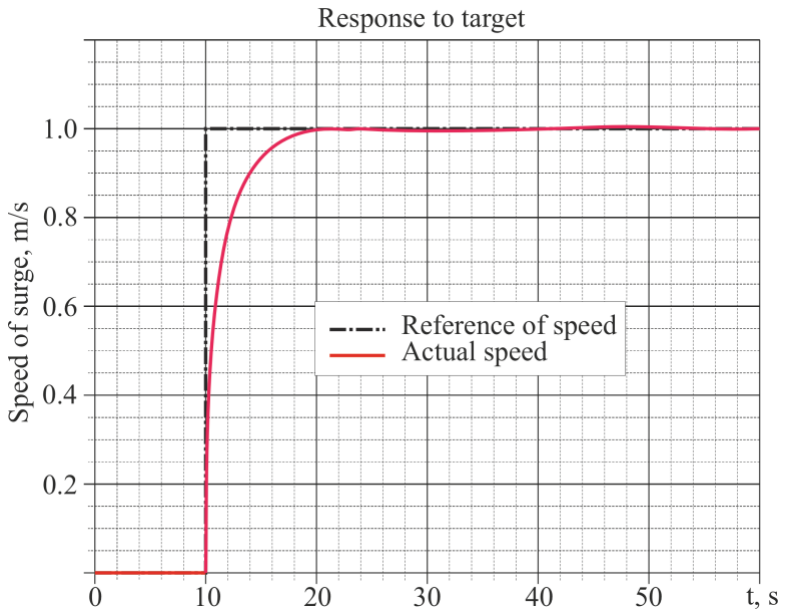

Fig. 10. Response to the jump in setting

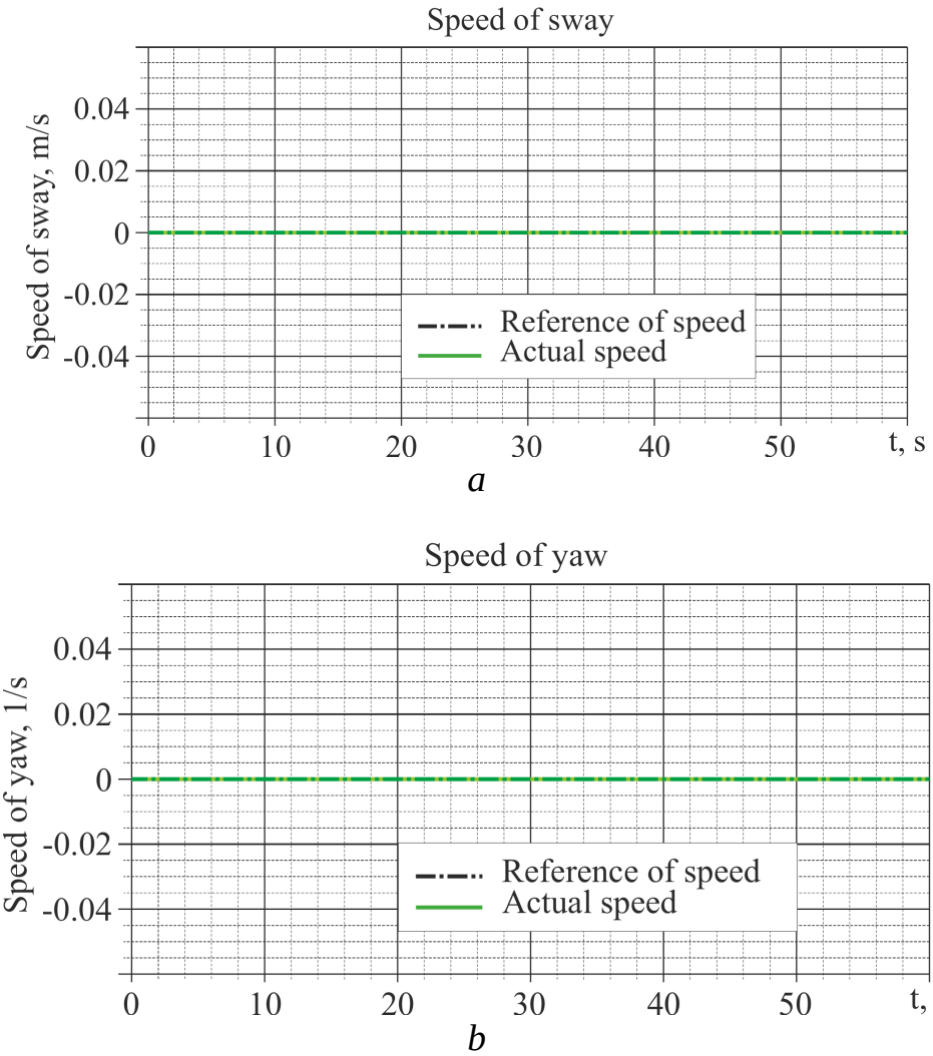

Fig. 11. Speed setting: *a* – sway speed; *b* – yaw speed

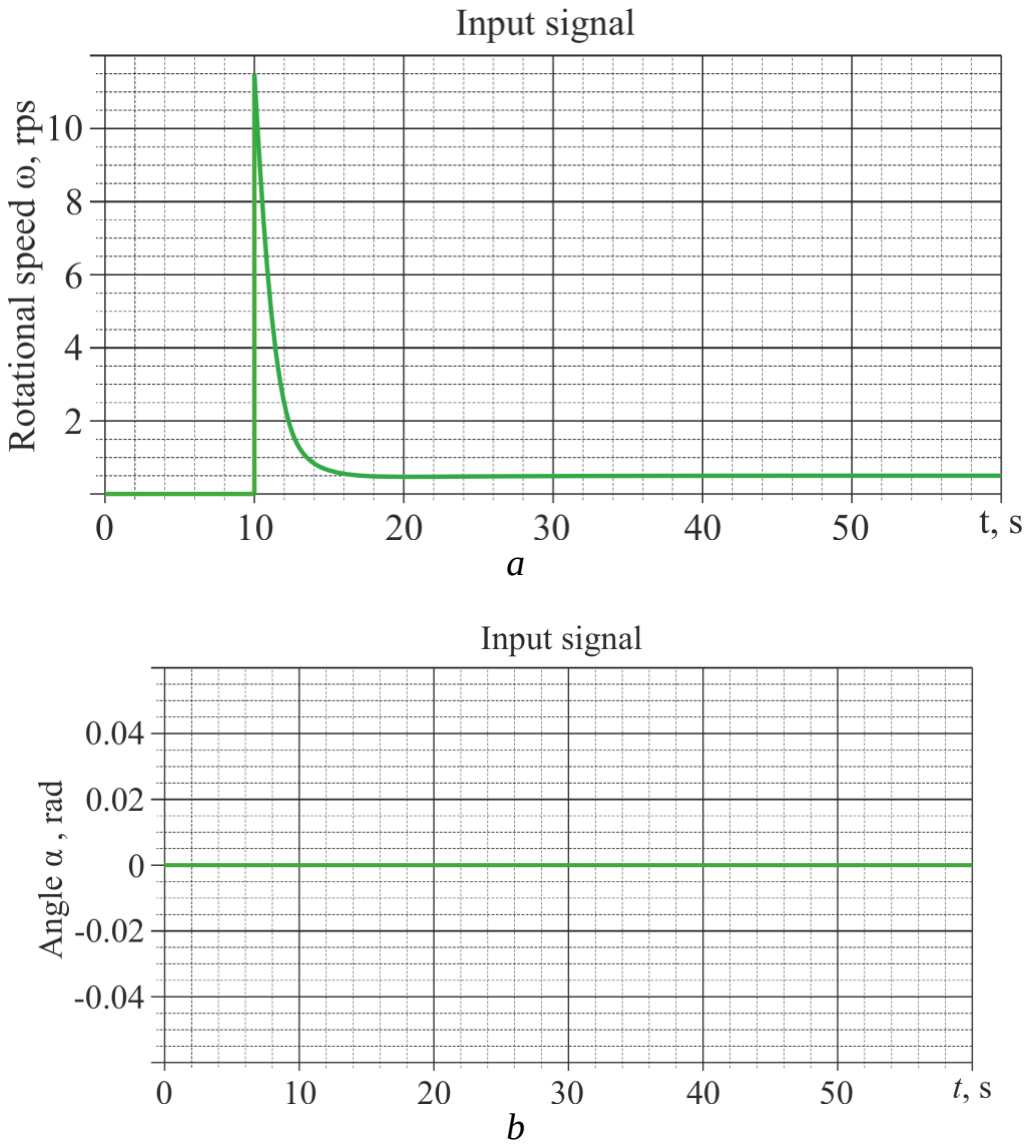

Fig. 12. Input signals: *a* – setting the speed jump; *b* – angle α

Fig. 12 demonstrates a jump in the speed of rotation (*a*), which stabilizes with a constant zero angle, which leads to a quick response to the jump and no overshooting. As expected, the reference zero angle does not lead to sway or yaw, as shown in Fig. 11.

5. 2. 2. Differential (asynchronous) control over azimuthal thrusters

For differential control, the goal was the same as for modeling synchronous control over ATs in order to get a quick response in response to perturbations. Thus, the setting was similar, with the exception of the bottom two elements in the left column of the reference amplification. They correspond to setting and must have different signs so that the controller can use them to stabilize the system. They can also be zero but then this simulation will be no different from a synchronous control simulation. In fact, this is not a problem, but it does not reveal the possibility of differential asynchronous control.

The simulation results are shown in Fig. 13–15. Some similar behaviors of the control system can be seen in Fig. 13, 14 compared to the previous modeling. This indicates that the simulation is working properly.

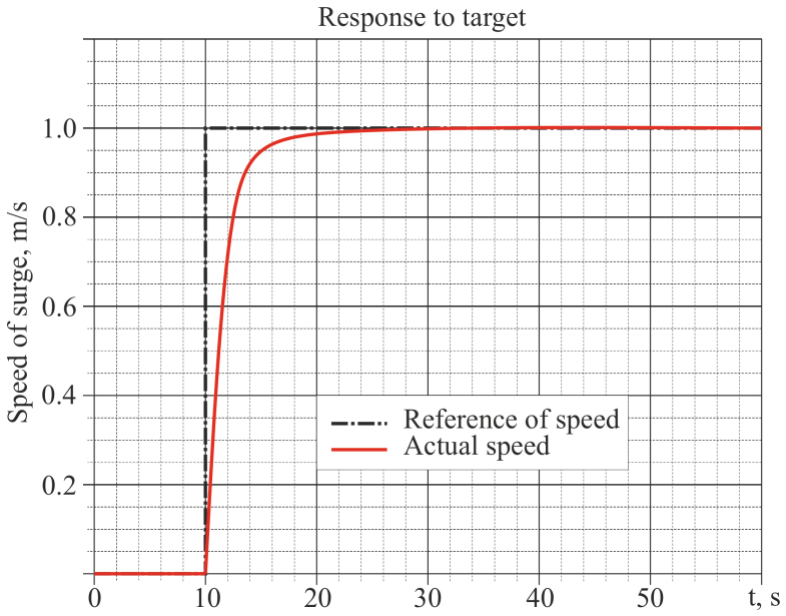

Fig. 13. Differential (asynchronous) response to the jump in setting

It can also be the result of linearization where the quadratic rotational speed function is more influential than the AT angle function. This may also be due to the fact that the elements of the matrix L_r (3, 1) and (4, 1) are not zero (59):

$$Q_1 = \begin{bmatrix} 120 & 0 & 0 \\ 0 & 1 & 0 \\ 0 & 0 & 1 \end{bmatrix}, Q_2 = \begin{bmatrix} 1 & 0 & 0 & 0 \\ 0 & 1 & 0 & 0 \\ 0 & 0 & 1 & 0 \\ 0 & 0 & 0 & 1 \end{bmatrix}, L_{r,p} = \begin{bmatrix} 8.03 & 0 & 0 \\ 8.03 & 0 & 0 \\ -0.015 & 0 & 0 \\ 0.015 & 0 & 0 \end{bmatrix}, \quad (59)$$

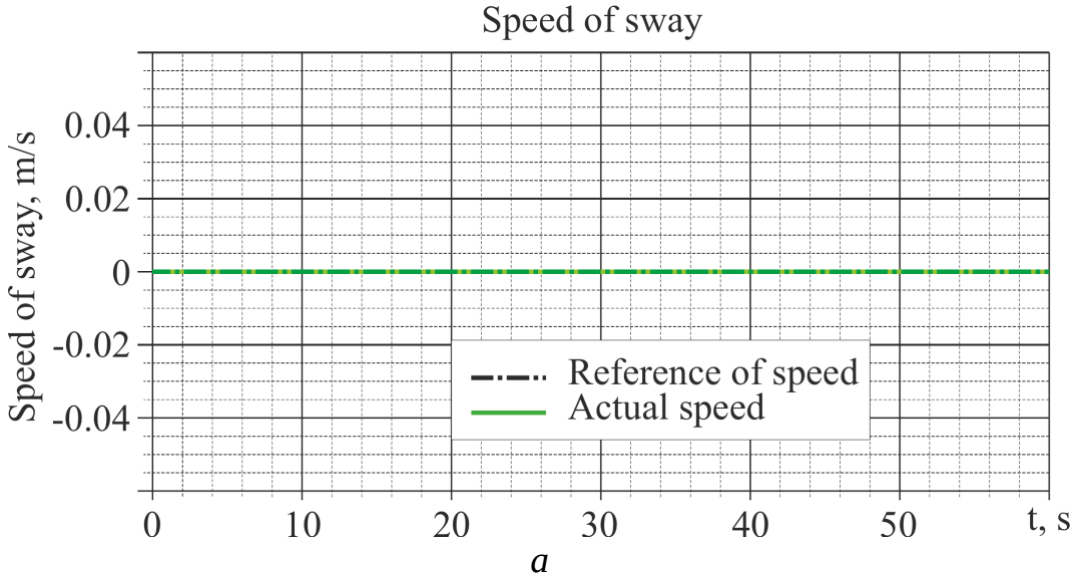

a

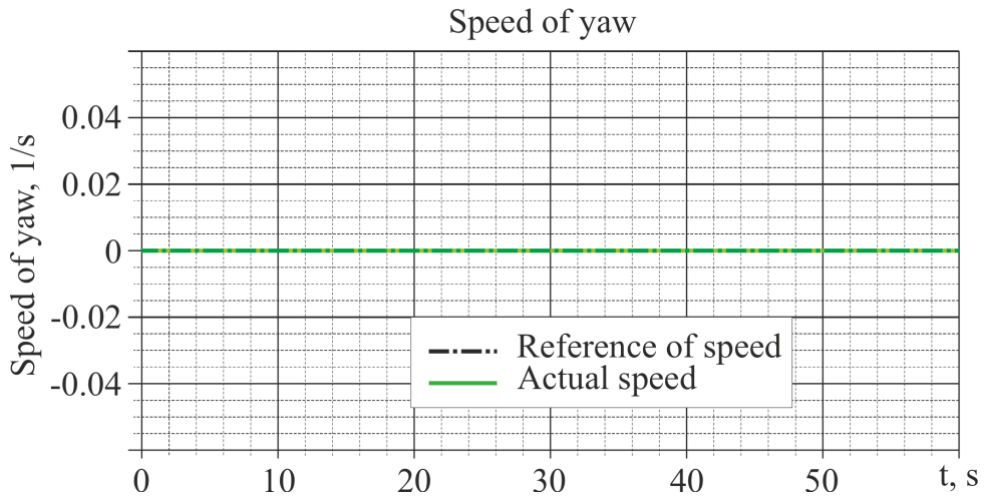

b

Fig. 14. Setting differential velocities: *a* – ~~drift~~ sway; *b* – yaw

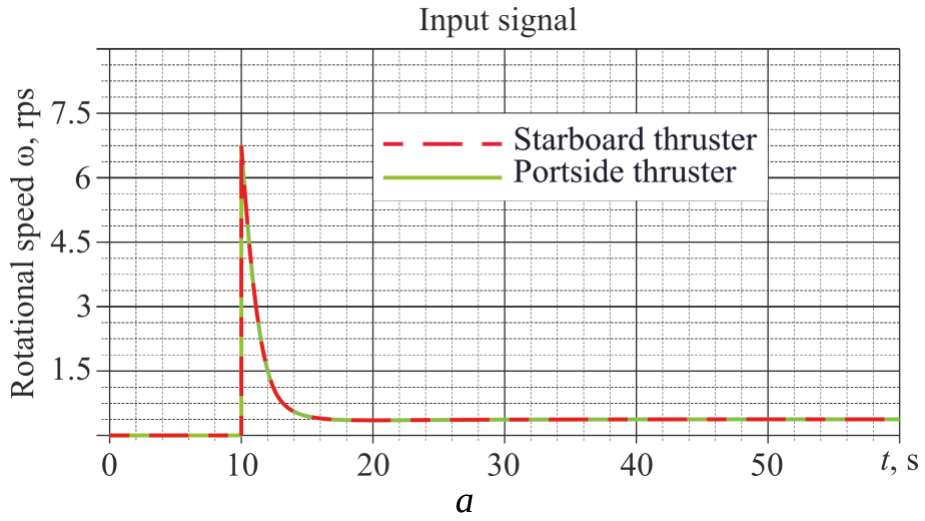

a

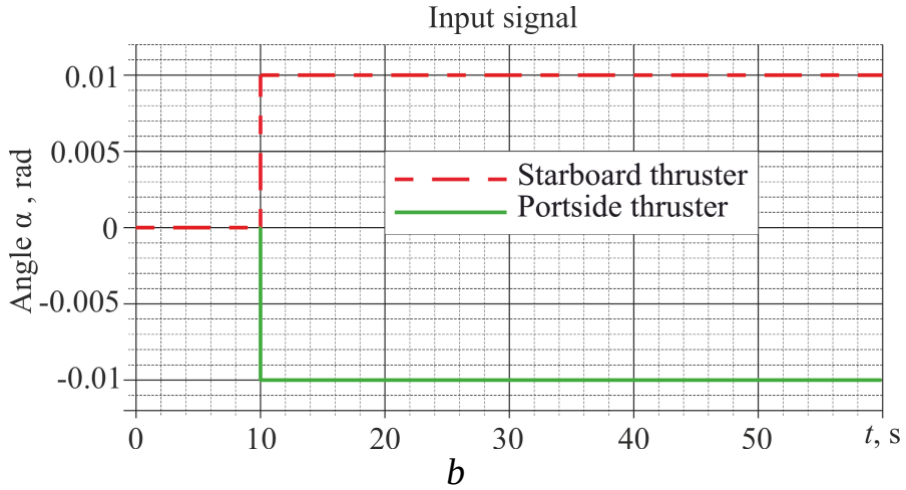

b

Fig. 15. Differential input signals: *a* – speed jump setting; *b* – setting angle α

Fig. 15 demonstrates some differences. Both engines have a small angle of location relative to the diametrical plane of the vessel. This leads to the fact that both AT engines need a lower rotational speed to ensure the assigned water flow rate.

5. 3. Yaw speed modeling based on a defined space of states

To investigate the behavior of the physical scale model of the vessel when turning, a step is taken to set the reference yaw speed. To test the possibilities and realistic implementation in practice, two different simulations are performed. One, in which there is some "mitigation" of the installation time and there is a re-adjustment (peak test), and another in which the controller tries to adhere to the reference task as "rigidly" as possible (smooth test). The peak test has been adjusted so that all simulations, including it, have the same installation time about 10 seconds after the start of the task. Since linearization and simplification of the model have been carried out, this test can give unrealistic results, but is still considered to correspond to the capabilities of the control system.

5. 3. 1. Zero-angle linearization with synchronous control

For subsequent simulations, the same rotational speed and angle of the propeller are selected for both ATs.

In this simulation, the controller uses matrices obtained by linearization around the operating point with translational motion of input signals (44), which are designed to work with the angle of the propeller close to zero. For the controller, two different settings are used, which are performed for two tasks: first, for the state when the input signals are equal to 1, and the reference gain is adjusted to achieve the target value. Another setting fixes a tracking error to increase rotational speed, providing the closest speed to the reference value while keeping the input level for a lower pitching speed value. In this regard, finding the limit of establishment takes more time, which gives information about the ability of the system by comparing a uniformly and more aggressively tuned system. Matrices of reference coefficients and transmission coefficients, where *p* and *s* denote peak and smoothing indices take the following forms, respectively:

$$Q_{1,p}=\begin{bmatrix}1&0&0\\0&1&0\\0&0&1\end{bmatrix},\ Q_{1,s}=\begin{bmatrix}1&0&0\\0&0.001&0\\0&0&200\end{bmatrix},$$

$$Q_{2,p}=\begin{bmatrix}1&0\\0&1\end{bmatrix},\ Q_{2,s}=\begin{bmatrix}1&0\\0&1\end{bmatrix},$$

$$L_{r,p}=\begin{bmatrix}0&0&1\\0&0&-22.4\end{bmatrix},\ L_{r,s}=\begin{bmatrix}0&0&1\\0&0&-14.06\end{bmatrix}. \qquad (60)$$

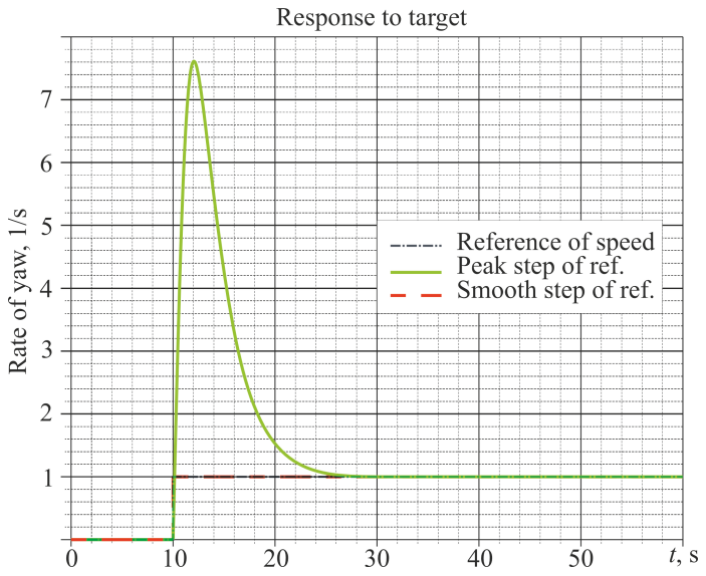

Fig. 16. Transitional characteristic of zero angle linearization

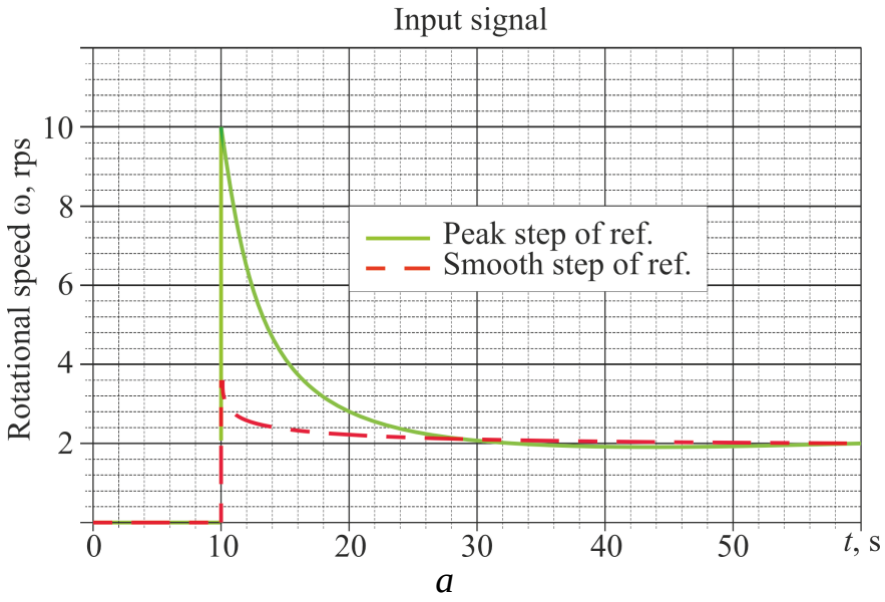

a

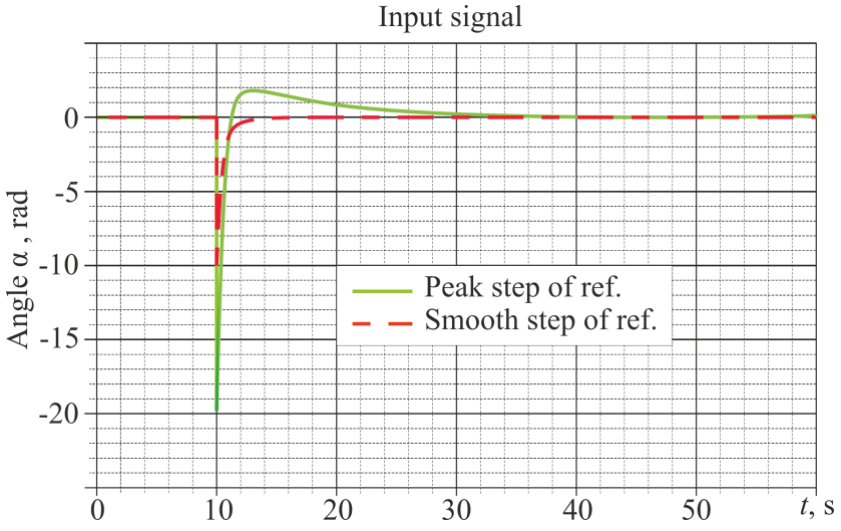

b

Fig. 17. Input signals of linearization of the zero angle: *a* – speed of rotation; *b* – angle α

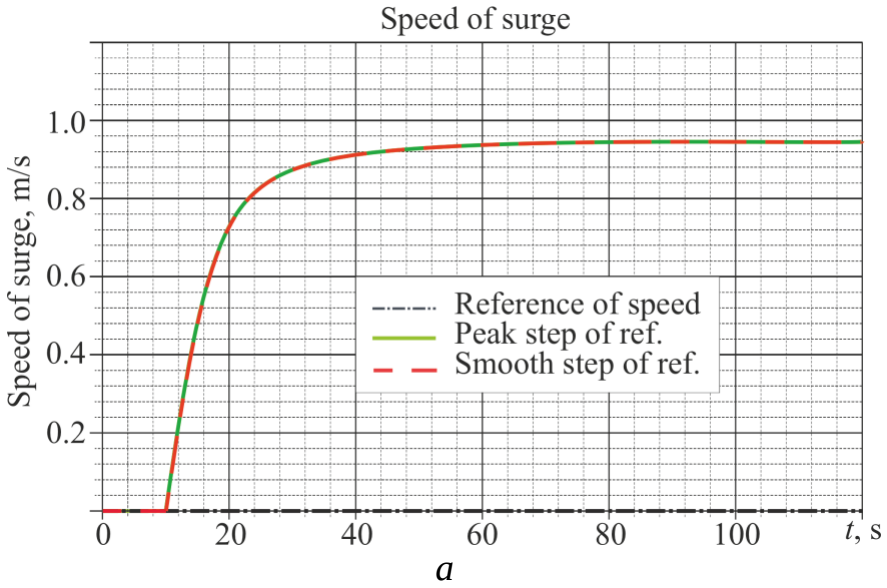

a

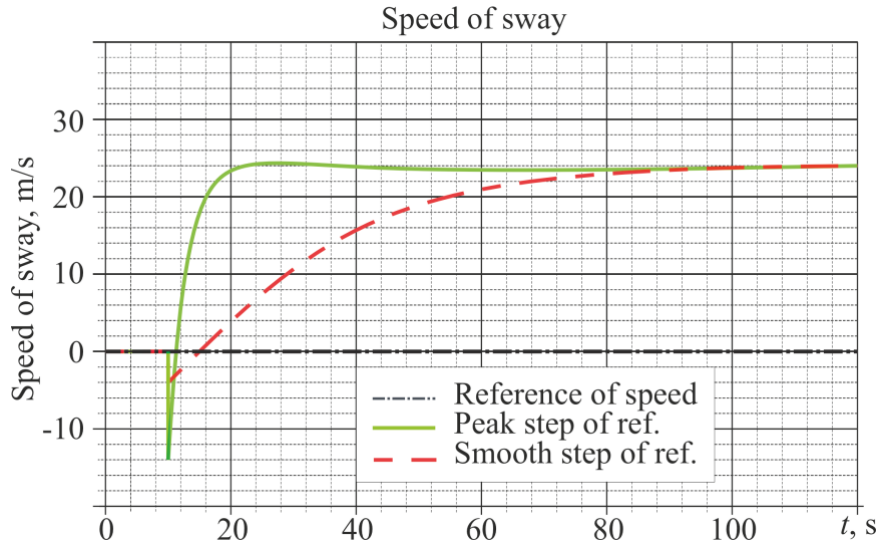

b

Fig. 18. Linearization at zero angle: *a* – speed of movement; *b* – ~~drift~~ sway speed

According to Fig. 17, *b*, the final value of α is $\alpha_p=\alpha_s=0.065$ rad.

Figure 16 shows the main results of the work of two different controllers. The maximum value setting controller provides an overshooting that is 7 times higher than the reference value but stabilizes after 10 s. Most likely, this is the result of a change in the angle of location of AT, as shown in Fig. 17, at which α reaches a very high negative value, close to –20 rad, which is far from a realistic scenario for a real AT. This fact gives reason to overestimate the need for a sharper change in the rate of yaw over the slow one to counteract the state when the overshoot reaches such a high value. However, reducing α is advisable from a physical point of view because a small negative angle will provide positive torque around the *z* axis and a positive yaw speed. Although it can be a debatable point if such a small angle can have such an impact if

the zero angle gives similar results for this controller mode. Another interesting aspect is how separated the rotational speed and speed throws are, since the controller shows the same behavior for both simulations, which for a real AT can significantly affect the results.

In a controller with a smooth setting, the output value seems to "follow" the reference value but differs from another controller. Reducing and restoring α to the final stabilized value occurs in less than a second, which is not possible for a real AT due to its dynamic properties. Figure 18 shows that the oscillation rate is set much slower. This means that there is some unrelated behavior since the input signal for the system is the same time interval of 20 seconds, but the oscillation rate at this time is different. Some unrealistic behavior of ATs may be associated with the linearization of α and its trigonometric dependence. The trigonometric function, which is periodic and only distributes the forces created by the number of revolutions between x_b and the y_b axis, cannot exceed 1. When applying linearization, the controller "believes" that the higher value of α corresponds to the higher value of the resulting force, which in practice is not true.

5. 3. 2. Linearization with nonzero angle in synchronous control

The model is configured based on the linearization method (45) where the angle of the propellers α has a small negative value, which is considered close to the resulting final value for a given simulation of the yaw speed. This is done in order to see if this setting will give better results than zero-angle linearization. The goals of designing settings are similar to previous simulations. One of the main differences is that the third element in the first line for the assigned gain value also needed to be adjusted. Otherwise, the speed jump tends to take a negative value, which requires a different behavior of the model and makes it difficult to compare the two simulations. The weight matrices and gain values for this simulation are as follows:

$$Q_{1,p}=\begin{bmatrix}1&0&0\\0&1&0\\0&0&1\end{bmatrix},\ Q_{1,s}=\begin{bmatrix}1&0&0\\0&0.0015&0\\0&0&225\end{bmatrix},$$

$$Q_{2,p}=\begin{bmatrix}1&0\\0&1\end{bmatrix},\ Q_{2,s}=\begin{bmatrix}1&0\\0&1\end{bmatrix},$$

$$L_{r,p}=\begin{bmatrix}0&0&10\\0&0&-21.6\end{bmatrix},\ L_{r,s}=\begin{bmatrix}0&0&3.63\\0&0&-14.09\end{bmatrix}, \quad (61)$$

which give the results shown in Fig. 19–21.

According to Fig. 20, the final value of α is $\alpha_p=\alpha_s=0.0168$ rad.

These results are similar to those obtained in the previous simulation but with some difference in the behavior of the model. The peak setting gives slightly better results since its overshoot only reaches a 6x reference value. The main difference lies in the higher speed of rotation of the propellers, which is almost ten times more influential on the speed of longitudinal advancement. That is, the non-minimal phase

response coincides with the fastest response when the maximum setting peak speed is reached. A smooth setting makes the controller's response slower than during the "peak setting" according to $Q_{1,s}$ (61).

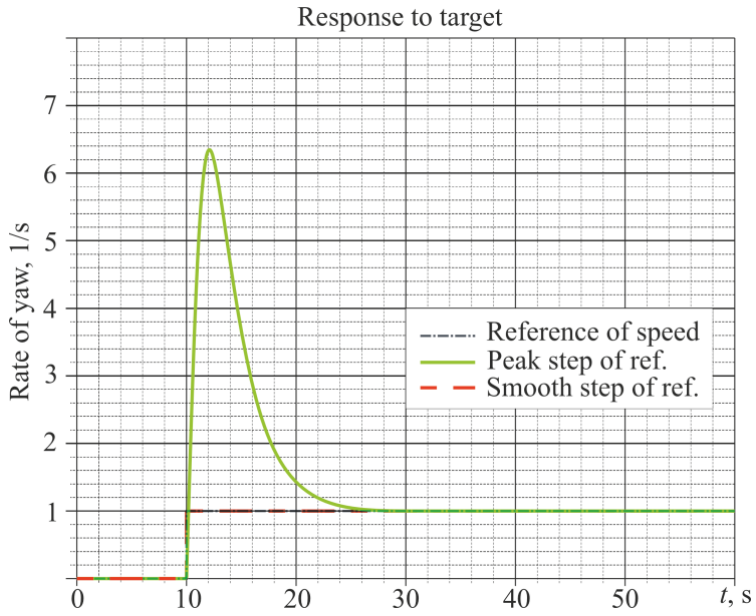

Fig. 19. Transitional characteristic with nonzero angle α

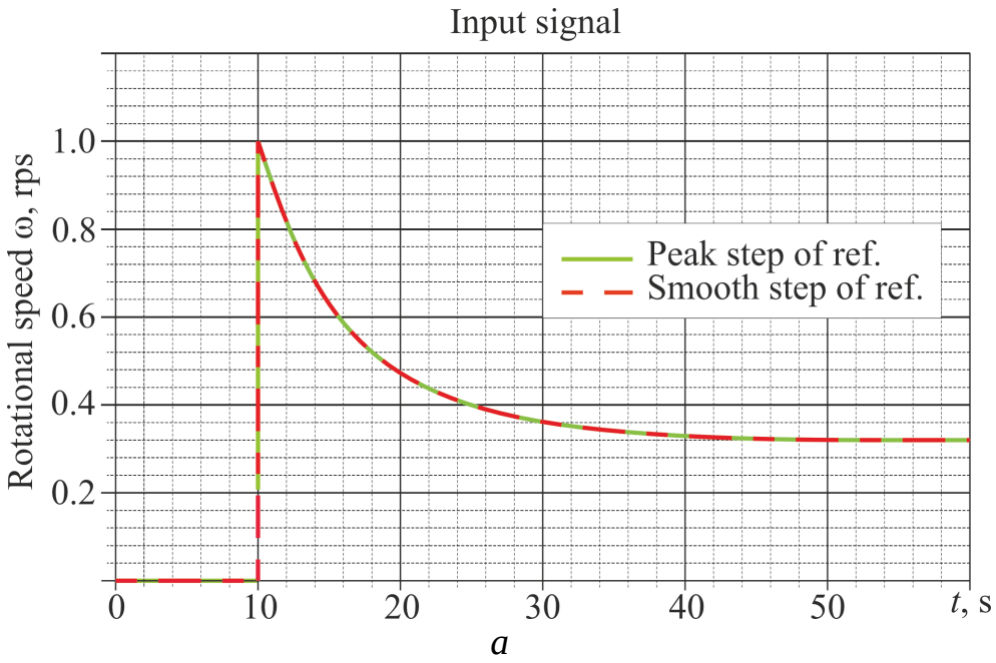

a

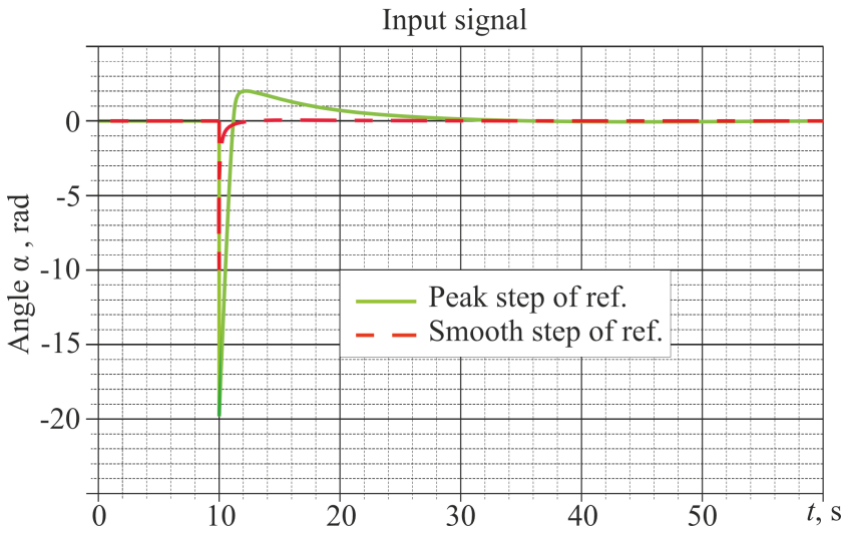

b

Fig. 20. Input signals with a non-zero angle α: *a* – propeller speed; *b* – angle α;

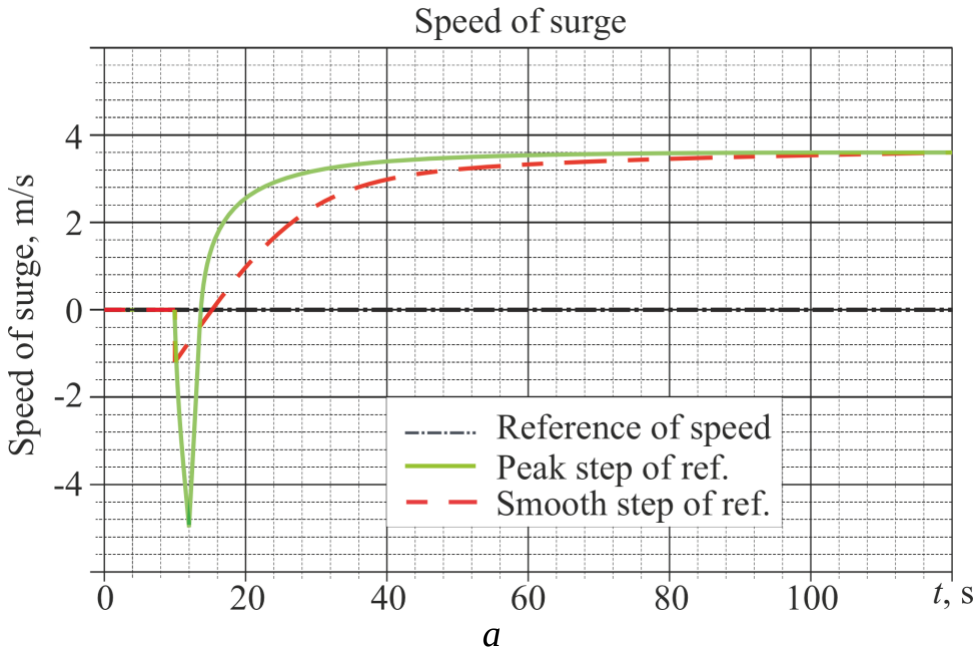

a

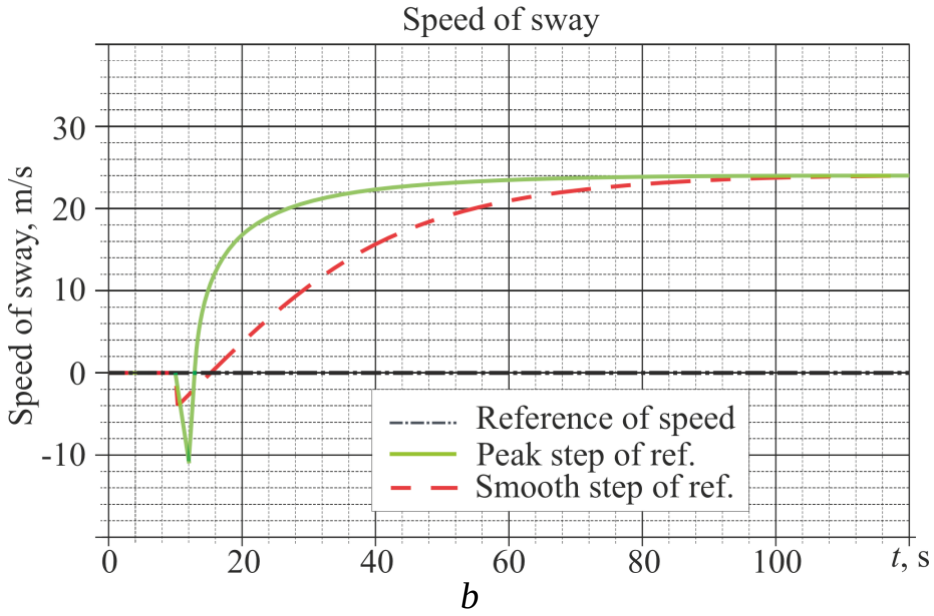

Fig. 21. Dependence of speeds with a non-zero angle α: *a* – speed of surge; *b* – sway speed

The most interesting thing in this simulation compared to the previous one is the charts of input signals in Fig. 20. The speed of rotation (Fig. 20, *a*) has *a* much greater value, in contrast to the angle α (Fig. 20, *b*), the resulting transitional characteristic of which has not changed much. First, it can be the result of linearization, in which the controller mainly responds to setting the angle α with the support ω at the same level if there is no need to increase the rotational speeds. Secondly, input signals show which setpoint values for α are positive, close to zero, but positive. Theoretically, for the modeling process, this should not be the case.

5. 4. Principles of linearization with independent control over rotational speed and angle of AT

5. 4. 1. Linearization with zero angle in asynchronous control

In the following simulation, differential control is applied, in other words, the possibility of independent control over the speed and angle of rotation of both ATs.

First, linearization with a zero angle α is used for differential (asynchronous) control over aft ATs. Modeling is carried out according to the same algorithm for the research of two configuration schemes for different purposes. Using differential (asynchronous) control, it is possible to observe a slightly different, potentially more improved behavior of the controller, which is confirmed by the following results.

$$Q_{1,p}=\begin{bmatrix}1&0&0\\0&1&0\\0&0&1\end{bmatrix},\quad Q_{1,s}=\begin{bmatrix}1&0&0\\0&0.015&0\\0&0&270\end{bmatrix},$$

$$Q_{2,p}=\begin{bmatrix}1&0&0&0\\0&1&0&0\\0&0&1&0\\0&0&0&1\end{bmatrix},\quad Q_{2,s}=\begin{bmatrix}1&0&0&0\\0&1&0&0\\0&0&1&0\\0&0&0&1\end{bmatrix},$$

$$L_{r,p}=\begin{bmatrix}0 & 0 & 1\\ 0 & 0 & 1\\ 0 & 0 & -20\\ 0 & 0 & -20\end{bmatrix},\quad L_{r,s}=\begin{bmatrix}0 & 0 & 1\\ 0 & 0 & 1\\ 0 & 0 & -12.32\\ 0 & 0 & -12.32\end{bmatrix}. \qquad (62)$$

The final values of α_p and α_s (Fig. 25) are: α_p=–0.084 rad, α_s=–0.41 rad.

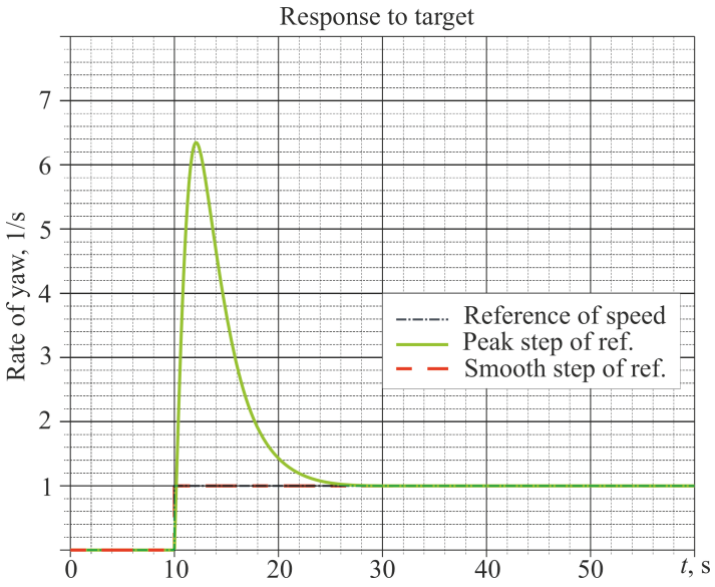

Fig. 22. Differential transition characteristic for the zero angle α

Transient characteristics for surge, sway, and yaw speeds (Fig. 22, 23) show the operation of ATs similar to the simulation of synchronous control in chapter 5. 3. 2. Here, the emission of the step characteristic is lower, and the speed of surge reaches a higher final value. However, some interesting things can be observed in the input signals. The angle α is the same for both engines with two different settings, despite the ATs having a differential degree of freedom. This may be the result of linearization, making it the only adequate solution. The great depression is shown in Fig. 25, while the simulation is smaller, indicating steps in the right direction. The final α value for the peak setting is almost similar to synchronous control but the smooth setting is closer to the actual π/6 value, which is also a good indicator for this controller.

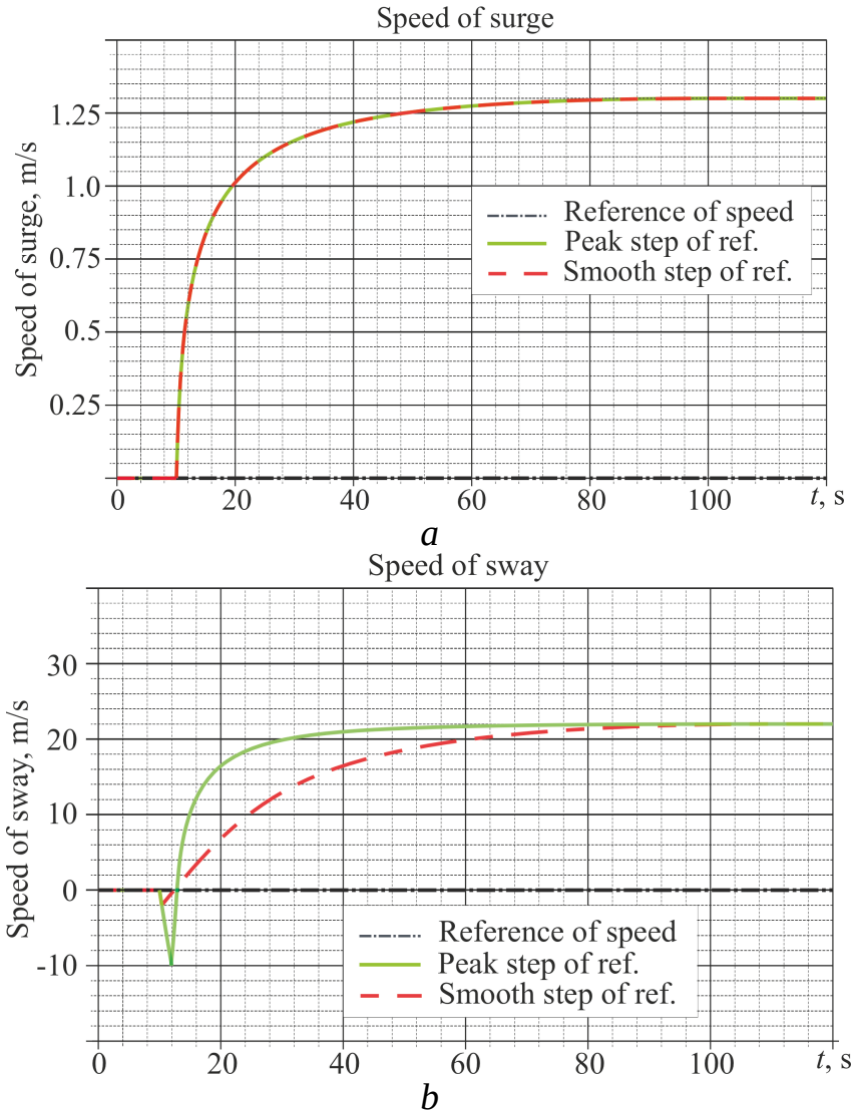

Fig. 23. Differential velocities at zero angle α: *a* – surge; *b* – sway

It is possible to observe completely different values of ω (Fig. 24), which indicates less impact on the system of this input signal. For both settings, one of the propellers rotates at a lower speed, which in practice is an advantage. When one propulsion provides more thrust, it creates the appropriate torque by turning the ship. Using this difference in rotational speed, the controller can more efficiently adjust the speed of rotation of the vessel.

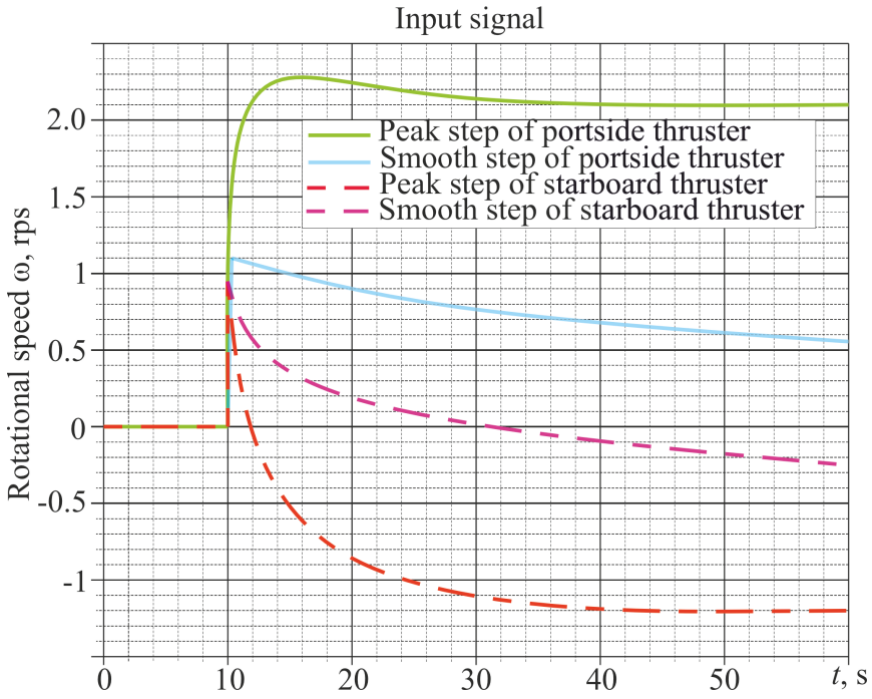

Fig. 24. Differential speeds of rotation of the azimuthal thruster at zero angle α

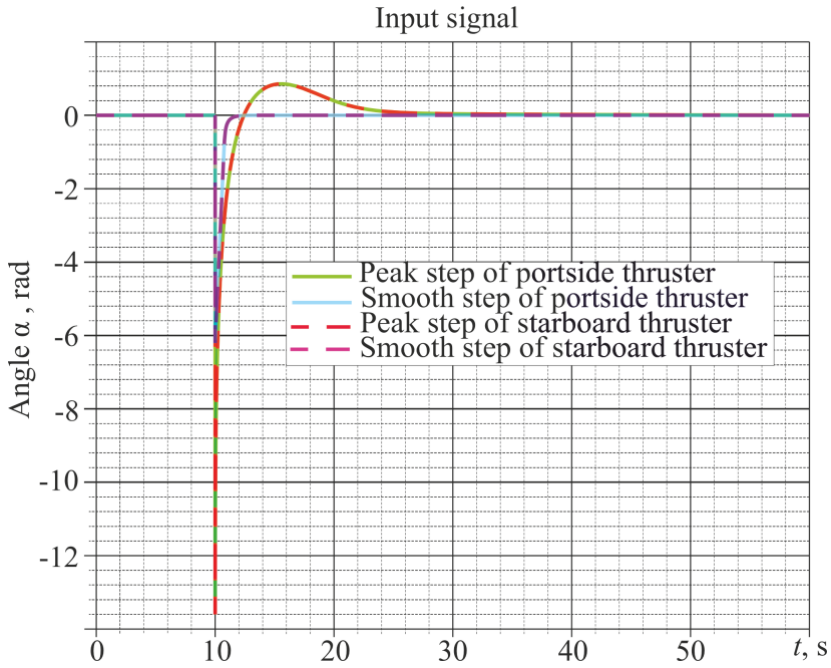

Fig. 25. Differential input signals at the assigned zero angle α

The problem that can be seen in this simulation is that any configuration of the values of the speed of rotation of ATs moves the ship "incorrectly". Since propulsion 1 is located to the left of the x_b axis, and propulsion 2 is on the right, this development will provide a negative rotation speed. This is another sign that the controller is counteracting itself, which confirms the consequence of the linearization of the input signal.

5. 4. 2. Linearization with a nonzero angle in asynchronous control

The following settings are based on a nonzero differential angle linearization model (45) and have the same adjustment aspects as in the previous simulation with the same problem where the controller required negative speed spikes. Therefore, this has also been fixed with the controller setup. Weight matrices and reference gain are as follows:

$$Q_{1,p}=\begin{bmatrix}1&0&0\\0&1&0\\0&0&1\end{bmatrix},\quad Q_{1,s}=\begin{bmatrix}1&0&0\\0&0.05&0\\0&0&250\end{bmatrix},$$

$$Q_{2,p}=\begin{bmatrix}1&0&0&0\\0&1&0&0\\0&0&1&0\\0&0&0&1\end{bmatrix},\quad Q_{2,s}=\begin{bmatrix}1&0&0&0\\0&1&0&0\\0&0&1&0\\0&0&0&1\end{bmatrix},$$

$$L_{r,p}=\begin{bmatrix}0&0&5\\0&0&5\\0&0&-5.31\\0&0&-5.31\end{bmatrix},\quad L_{r,s}=\begin{bmatrix}0&0&5\\0&0&5\\0&0&-5.31\\0&0&-5.31\end{bmatrix}. \qquad (63)$$

The simulation results are shown in Fig. 26–29.

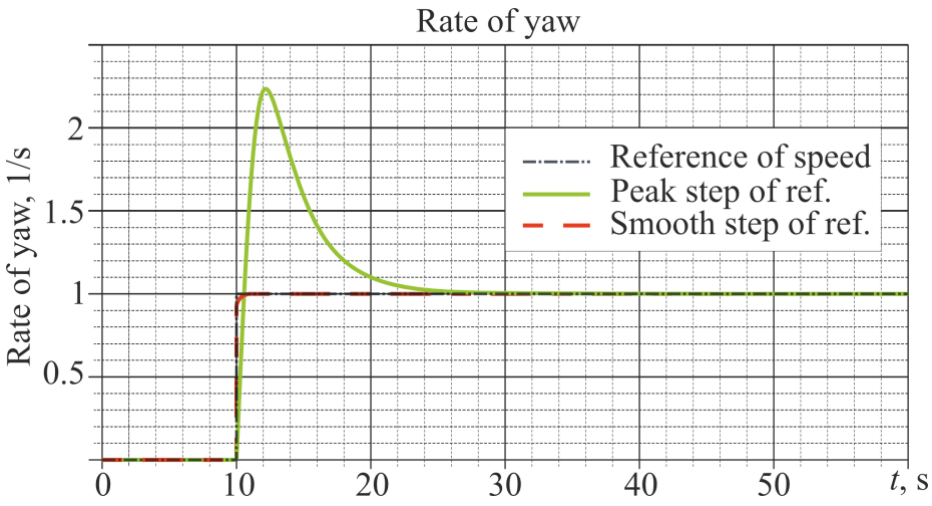

Fig. 26. Differential transition characteristic with a nonzero angle α

The final values of α_p and α_s (Fig. 29) are equal to:

$\alpha_{p,1}$=3.64 rad, $\alpha_{s,1}$=2.68 rad,

$\alpha_{p,2}$=−4.81 rad, $\alpha_{s,2}$=−3.52 rad.

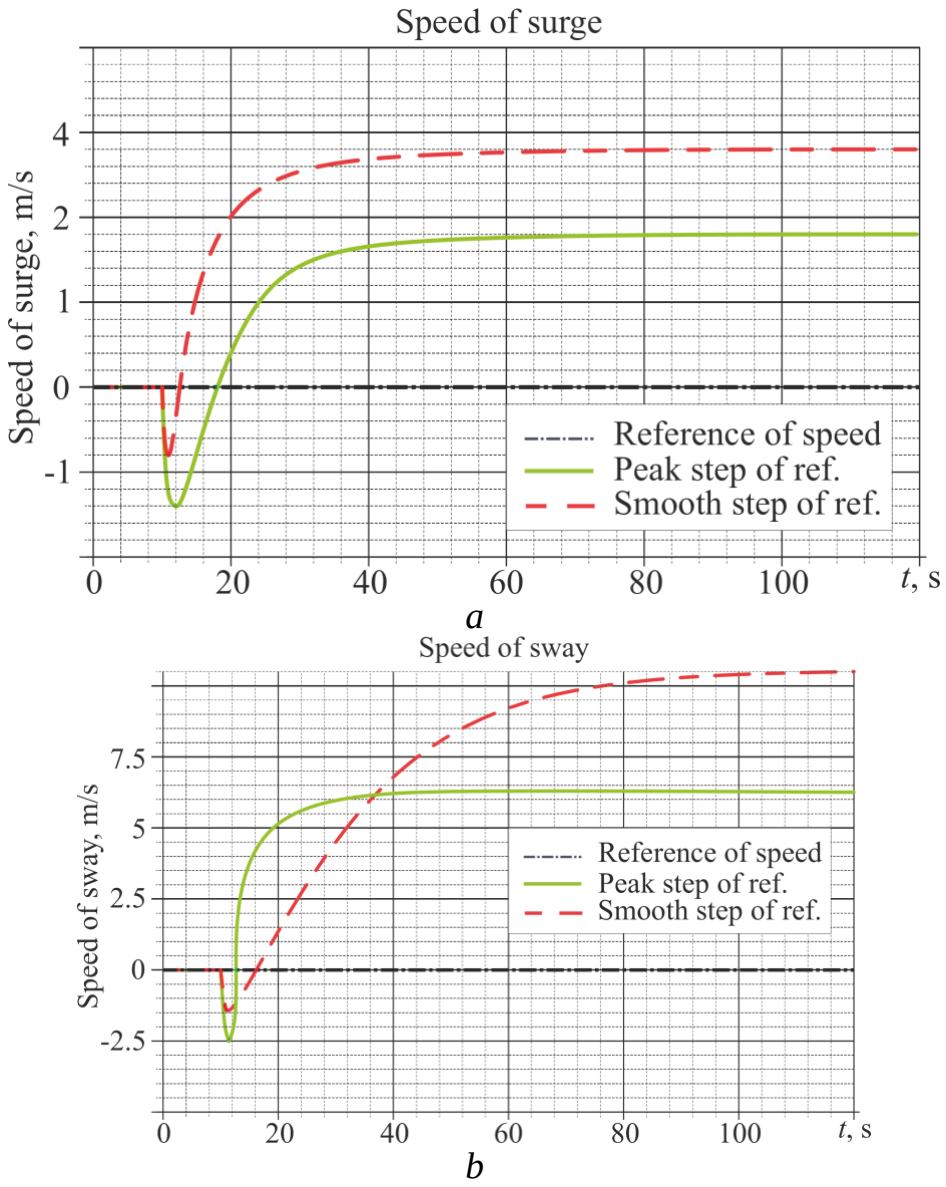

Fig. 27. Differential velocities at a nonzero angle α: *a* – surge: *b* – sway

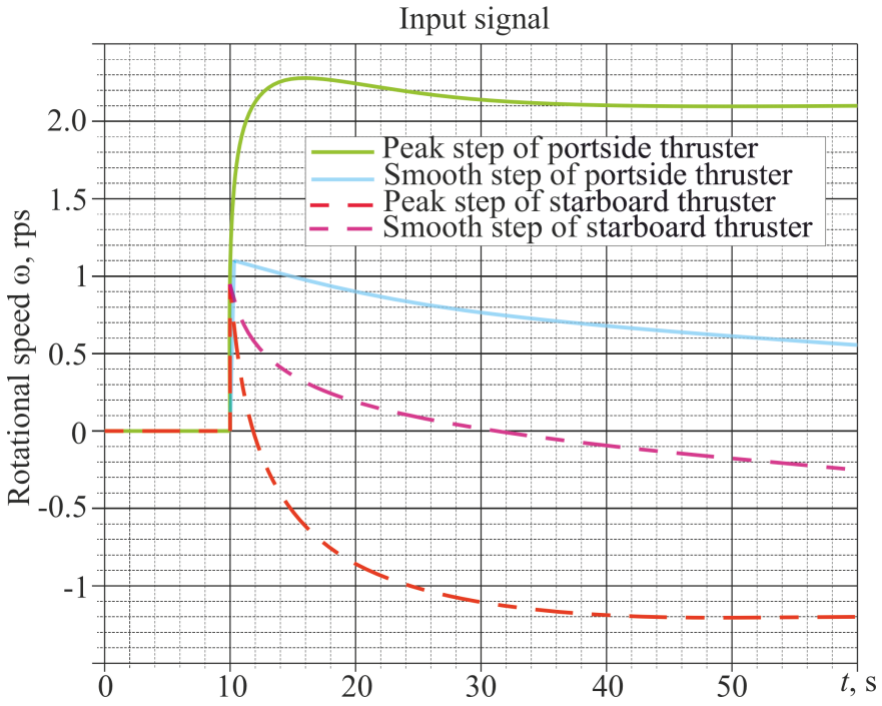

Fig. 28. Differential rotational speeds with a nonzero angle

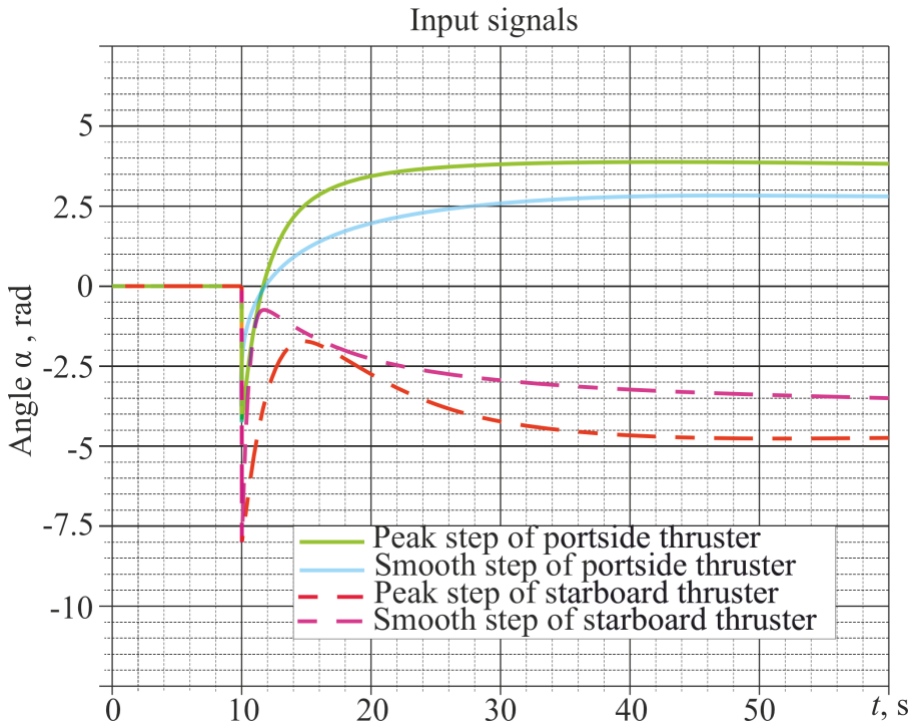

Fig. 29. Differential input signals at the assigned nonzero angle α

The simulation results are unique from all yaw velocity simulations. The peak step shows that the emission is significantly lower than in any of the previous calculations. This excess reaches only double the value in relation to the reference. Charts of transients in Fig. 29 demonstrate results similar to previous simulations but with different final values. They can be configured through the application of reference amplification, which is not necessary because the purpose of the simulation is to find

out how the behavior of ATs affects the system, and not what are the final values of the angles α.

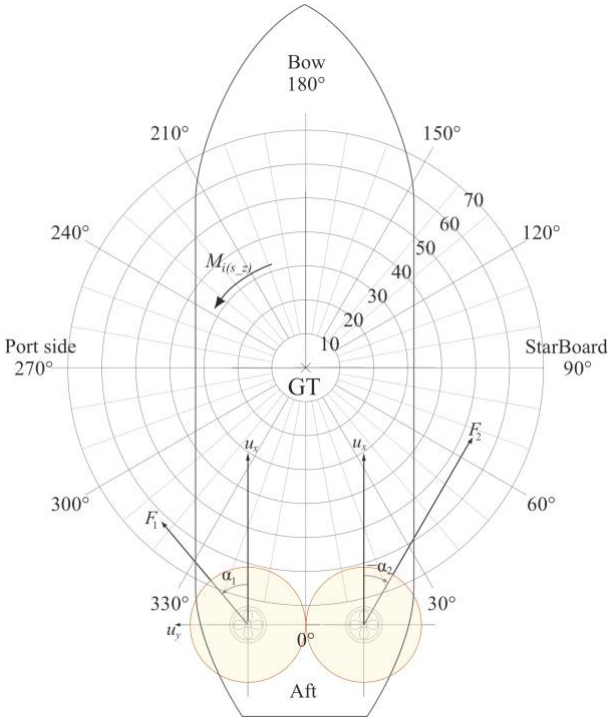

Fig. 30. Illustration of differential modeling results with the angle α different from zero

However, in practice, input signals "behave" realistically. Both the jump settings and the smooth setup lead to similar transient characteristics but with different final values. These values have been interpreted and illustrated in Fig. 30, which shows that both ATs engines, as in previous simulations, are counteracting each other but now in a controlled way. The left AT has a greater angle α value compared to the right, which provides more torque around the *z* axis and, therefore, an increase in rotational speed. Although the right motor has a higher rotational speed, creating negative torque around the *z* axis and thus canceling the forces from the left motor. This makes it possible to achieve a constant turning speed. However, the method creates many unnecessary opposing forces in the direction y_b. Angle values are still far from the operating point, making linearization accuracy low. However, our results show trends in the right direction.

5. 5. Determining the limiting characteristics of the controller

To ensure more efficient and reliable control, it is necessary to ensure adequate real-time distribution of ATs thrust and the generation of optimal control input data, namely rotational speed and azimuthal angles. To do this, LQR must use a sparse matrix structure using the variable direction method of the multipliers to obtain a reliable optimal solution.

To partially solve this problem and further improve the system, an algorithm was developed to establish limits of azimuthal angles instead of strictly observing the

reference step of the yaw velocity. This simulation was performed with differential nonzero angular linearization. The matrices of weight and reference gain for this simulation are as follows:

$$Q_1 = \begin{bmatrix} 0.01 & 0 & 0 \\ 0 & 0.01 & 0 \\ 0 & 0 & 1 \end{bmatrix}, \quad Q_2 = \begin{bmatrix} 1 & 0 \\ 0 & 1 \end{bmatrix},$$

$$L_r = \begin{bmatrix} 0 & 0 & 6 \\ 0 & 0 & 6 \\ 0 & 0 & -1.31 \\ 0 & 0 & -1.31 \end{bmatrix}. \qquad (64)$$

The simulation results are shown in Fig. 31–34.
The final values of α_1 and α_2 (Fig. 34) are: α_1=0.63 rad, α_2=−0.28 rad.

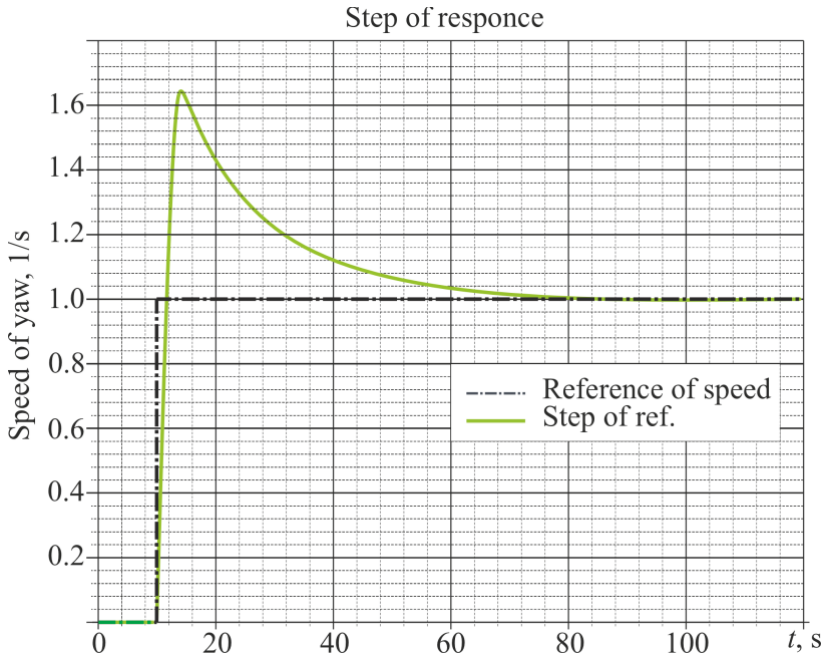

Fig. 31. Setting a step-by-step characterization limit

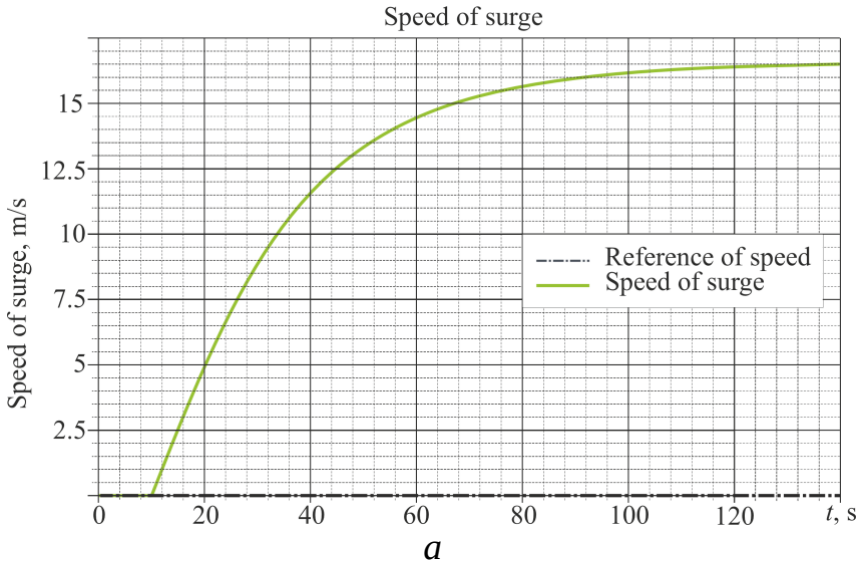

a

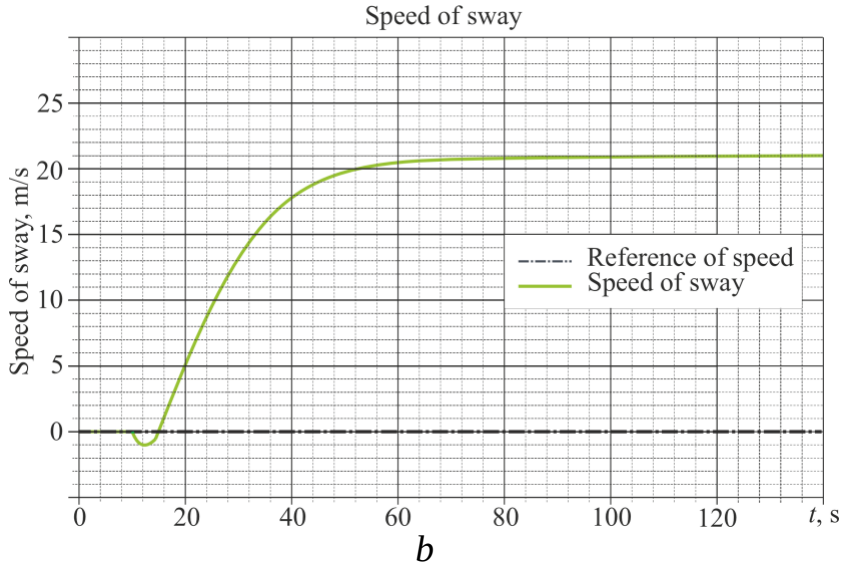

b

Fig. 32. Restriction settings: *a* – acceleration of surge; *b* – acceleration of sway

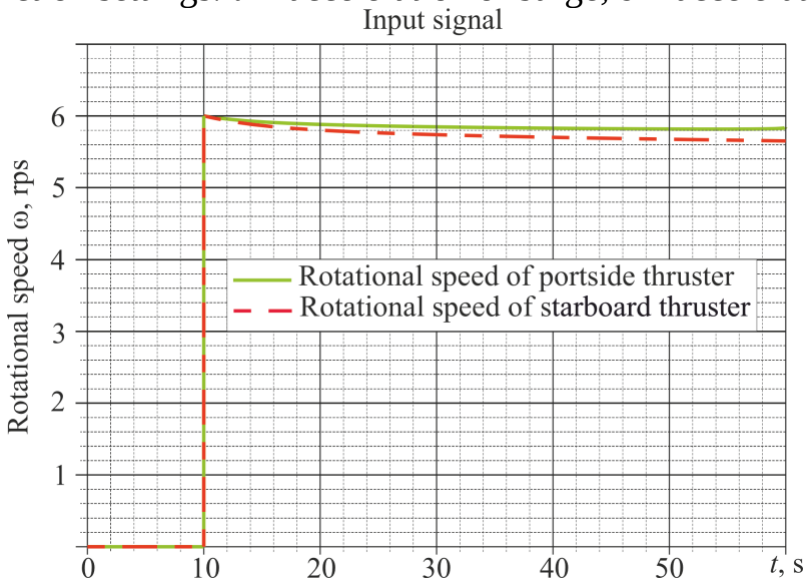

Fig. 33. Setting the rotational speed limit

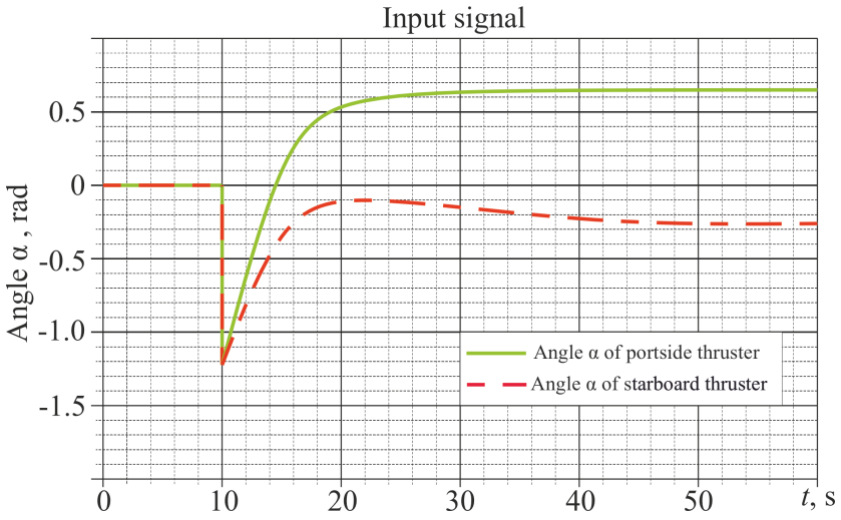

Fig. 34. Setting an angle α limitation

The result of this simulation gives the lowest jump in setting the angle α of all previous simulations but instead has a much longer establishment time, reaching almost a minute. The acceleration speed of surge is also significantly greater than in any previous simulation. This simulation assumes that the appropriate configuration of the controller for the model will be longer, which indicates a non-significant decrease in the versatility of the controller by increasing its prospects.

When compared with a possible real reaction, almost any angle α that is not close to the working value will differ significantly from the actual one. A possible solution for this problem is to use predictive amplification.

Predictive amplification is an approach to controlling a nonlinear system using multiple linear controllers. Thus, having several linearization species with respect to the approximation of the trigonometric function at different operating points, LQR can be applied to these segments independently.

The use of predictive LQR gain can help eliminate the problem of switching between linearization species. If we neglect this aspect, then an unstable state or instability in the system may occur.

Table 1 gives the calculated data and parameters of the physical model of SBVs (Fig. 1–5) for real-time modeling of the model's behavior in dynamic positioning mode with adequate distribution of ATs thrust and the generation of optimal control input data.

Table 1

Parameters of the SBV model and thrusters

Name	Designation	Unit of measure	Value
Port side AT	Δ_{y1}	m	–1.22
	Δ_{x1}	m	–0.23
	$F_{\max}$	N	894
	$F_{\min}$	N	0.264

	ω	r/s	7.96
	α_{1max}	rad	3.925
	α_{1min}	rad	–0.785
	Δα	rad	0.088
	M_p (56)	N/(r/s)^2	6.6e-4
Starboard AT	Δ_{x2}	m	0.23
	α_{2max}	rad	–0:175
	α_{2min}	rad	–3:054

The SBV model with ATs moved forward with a constant thrust force F_x, and changed course by turning the moment, changing in time lasting 450 s. Random "noise" was added to the desired generalized force (Fig. 35, *c*) to check the reliability and constancy of the assigned method of thrust distribution.

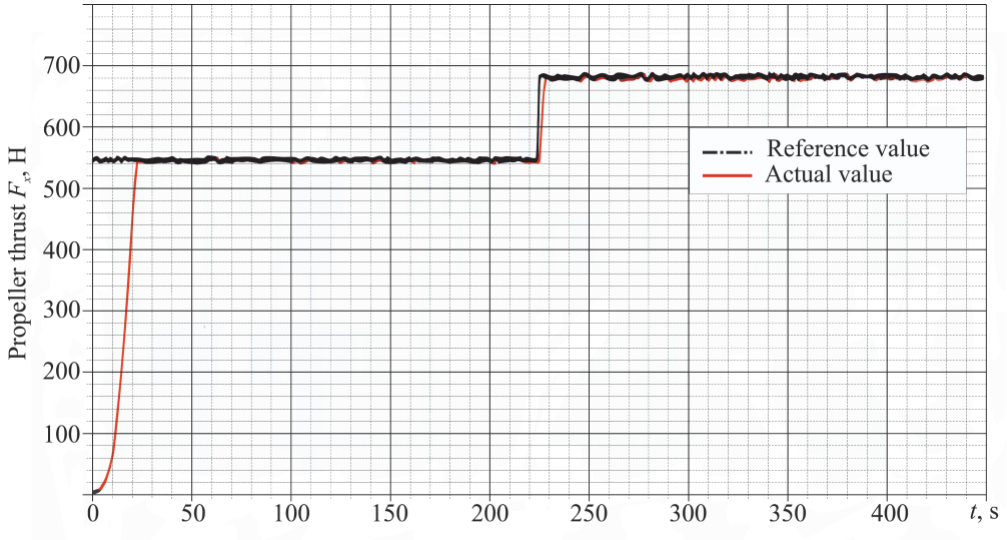

a

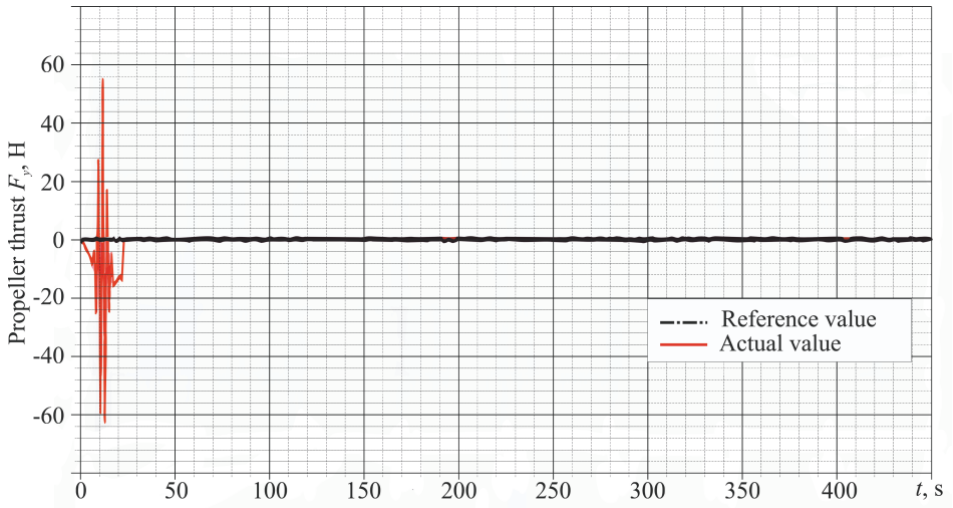

b

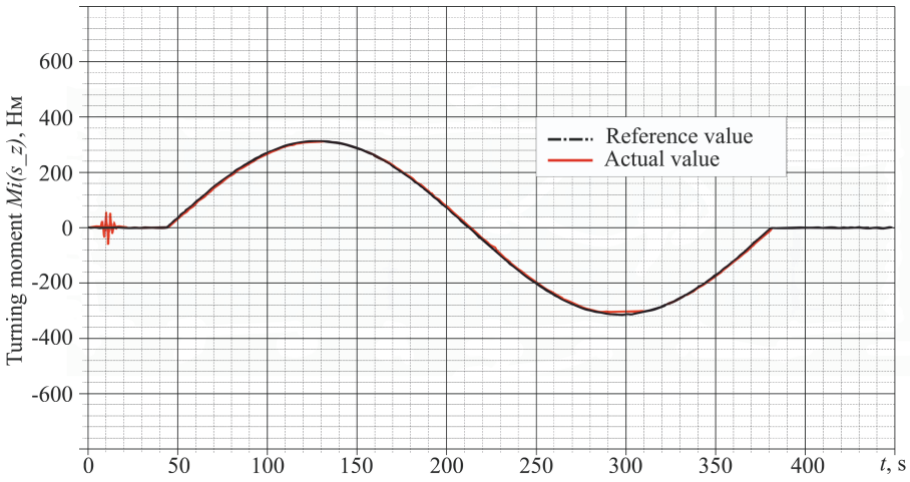

c

Fig. 35. Real-time simulation results: *a* – propeller thrust characteristic F_x; *b* – characteristic of the thrust of the propeller; *c* – F_y, characteristic of turning moment

It is shown that the real value of the generalized force is well consistent with the assigned generalized force, except for the duration of the time from 0 to 25 s where a rapid increase in F_x leads to a deviation of F_y.

6. Discussion of the results of researching the method of linear-quadratic control over the physical model of a vessel with azimuthal thrusters

Based on the simulation results, we can conclude that the functional ability of the controller relative to the real situation depends primarily on the configuration of the values of the speed of rotation of ATs. The problems that arise with the controller and model, and possible potential solutions to improve the system as a whole, rely on the LQR predictive gain method, which in turn will help eliminate the problem of switching between linearization species.

When modeling the acceleration of surge, the results show adequate operation of the controller, which quickly works out the task without a significant difference between synchronous and asynchronous (differential) control of aft ATs. The relationship between the speed of rotation of the propeller and the actual speed of the model is linear, which can be considered an excessive simplification. Performing additional physical tests of the model in terms of determining the true nature of such a dependence, it was found that the resulting model can improve the characteristics of the controller when modeling the yaw speed. Another interesting thing that could be tested is the work of the controller under the influence of non-deterministic environmental disturbances, such as wind, waves, or currents. This can be done in research pools with the appropriate equipment.

When modeling the yaw speed, the results showed the true capabilities of the model and controller since they included all states and input signals. The two settings, one of which "hard" tracked the set speed and the other was somewhat "softer" in the time of reaching the setpoint, had mostly the same dependence of the output signal (Fig. 17, 20). Some interesting results regarding the ratios of the maximum and final values of the angle α can be observed for the dependences of input signals and the

velocities of surge/sway (Fig. 23, 27). For all simulations and settings, the azimuthal angle reached a relatively large negative value before reaching a steady one.

In practice, this will force the AT engines to rotate around the axis of the baller, increasing the yaw speed, which, from the point of view of the characteristics of the controller, occurs due to the linearization of the model, or rather by controlling the angle α and linearization of the input signal. Excessive dependence on the angle α means that it is effectively possible to control only the angle of α, and for the overall control over the movement of the vessel, more delicate adjustments are required. Excessive dependence on the angle α is observed on the dependences of surge and sway. Here, the speed of surge is much lower than the sway speed, which means that the vessel is moving mainly by lag, which in practice under this mode would create resistance and stop. To continue moving, it is necessary to change the orientation of the vessel. When simulating pitching, the risk of overturning the vessel also increases. This indicates that something is amiss with the model and is most likely the result of the simplifications made during the creation of the model.

Most of the elements in the matrix of states A (53) are zero, which in practice would have a great impact on a real vessel during physical tests. These elements show how much some states depend on others and to what extent. "Zero" elements indicate that there is no relationship between these states – centripetal forces and Coriolis forces. However, it is the linearization of the input signal that leads to the reaction of the controller, which is not fully adequate with respect to the actual change in the angle α of ATs. Thus, to resolve the specified discrepancy between the input signals and the output forces of ATs, additional research is needed, in particular in the area of changing the differential settings of the controller.

The speed of rotation of the propellers is different for two ATs, which makes it possible to change the direction of movement of the vessel without changing the angles α of ATs. During the simulation, the controller sets the speed of rotation of the propellers in such a way that a negative yaw velocity is created, so that it counteracts the change in the input angle. This can also be the result of excessive dependence on the angle α, so the speed of rotation of ATs propellers is used only to obtain the exact result corresponding to the task. However, the last simulation, which is a differential (asynchronous) control with linearization of a nonzero angle, is the most physically probable scenario (Fig. 30). The right AT pushes the ship forward and right, and the left AT, if continued to turn in said direction, will also create a greater emphasis for the vessel to turn right. This shows that the applied principle of control creates many opposing forces directed in different directions, which physically indicates the adequacy of the solution and the potential feasibility of using this control method.

Modeling a mode under which the speeds of surge, sway, and yaw are less dependent on each other also creates several problems with the control of the vessel, for which it is necessary to improve the theoretical part of the simulation in order. For example, centripetal and Coriolis terms, $C_{RB}(\nu)$ must be linearized using different stationary points. The damping matrix $D(\nu)$ here is approximated by a diagonal matrix but could potentially be expanded, which as a result could be the cause of an unrelated vessel reaction in a particular state. The values of the parameters can affect the negative simulation result. Therefore, operational tests with monitoring of the parameters of

certain measured resistances and azimuthal characteristics can help improve modeling performance.

ATs are characterized by extremely high force intensity of the elements of their design. Mechanical loads can reach the permissible limit of strength. First of all, this applies to the elements of Ats subjected to the most intense influence of operational loads and the corresponding destructive processes. Exaggeration of loads beyond nominal causes destruction of the installation elements. In combination with the absence of reserved parts and assemblies in ATs, the destruction of any main element leads to a loss of operability of the installation at all. Information about the load in the elements of ATs can be used as an additional one in the implementation of the installation control processes. The conclusion is based on the assumption that a change in geometry or a decrease in the damping of vibrations by the supports of ATs elements should be reflected in the total load transmitted by the propeller and PEM to the hull of the vessel in the support placement brackets. Therefore, it is advisable to use as additional information the results of incliniometry of PEM supports [36, 37].

The limitation of our studies concerns primarily achieving the consistency of additional measurements of perturbations in the cases where the moments of the first order are unknown. In this case, a structure is proposed for estimating the moments of the first and second order along with the parameters of the model. Secondly, theoretically, the time of increase in torque in FC with PWM is limited by the inductance of the motor in dependent current inverters with a DC link. This aspect requires experiments on parameterization, which is not always possible.

The disadvantages of this research include the fact that in order to take into account these restrictions, a number of simplifications were adopted:

– we excluded degrees of freedom (DOF), which have little effect on the system;

– only 3 degrees of freedom (DOF) out of 6 (pitching, roll, and yaw) were used in the simulation;

– some parts of the resulting mathematical model were linearized to make the model work with LQR.

To solve these problems and limitations in terms of obtaining more adequate results, instead of using the LQR infrastructure, which requires linearization, it is necessary to apply a method based on a model predictive controller (MPC), which eliminates the need for linearization. Since MPC is also based on the theoretical models discussed in this research, they can be reused. Another option for controlling the vessel may be to use Fuzzy LQR, which can handle nonlinear systems [38–42].

The practical significance of our results is the fact that the quadratic optimization model is a very effective and reliable technique in the process of designing sea-based vehicles of various configurations of thrusters for optimal control.

Owing to its low computing complexity and hardware requirements, control distribution algorithms can work on embedded platforms. In addition, it is possible to apply averaged values to the control commands for ATs engines, which leads to a decrease in the wear of structural elements.

7. Conclusions

1. For the physical scale model of SBVs, the physical model of ATs in the aft part can be implemented on the basis of actuators, an electronically commutated motor, and a servo drive for each AT. Electronically commutated motor is connected to the propeller of AT through gear transmissions. In practice, the controller uses input data from GPS and IMU to determine the position, course, and speed of the vessel. To adjust the speed and torque of the electric motor, it is necessary to measure the currents of the motor and calculate the throughput of converters with high accuracy. In practice, it is necessary to provide for limiting the rate of change of torque to prevent damage to the mechanical part of the electric drive.

2. Checking the behavior of the model showed that in order to obtain a relatively fast transient characteristic with minimal overshooting, it is necessary to minimize the tracking error. Studies of the design features of vessels of this class confirm that jumps in the speed of rotation of ATs, which stabilize with a constant zero angle, lead to a quick response to the jump and the absence of overshooting. The small angles of location of ATs relative to the diametrical plane of the vessel lead to the fact that both AT engines need a lower rotational speed to ensure the assigned water flow rate.

3. The determination of the space of states and the linearization of ATs control system allows for adequate modeling of the yaw velocity to track the effect of disturbing forces on the characteristics of the controller. Moreover, it was found that small negative angles provide positive torque around the *z* axis and a positive yaw speed. To take into account the dynamic properties of real ATs, it is necessary to be able to adjust the reduction and restoration of angle α to the final stabilized value. It can also be concluded that when applying linearization, the higher value of α corresponds to the higher value of the resulting force, which in practice is not true.

4. Independent control over the speed and angle of ATs with linearization with zero or non-zero angle of ATs proved its greater adjustable ability than synchronous. To reduce the counteraction of ATs engines, it is necessary to apply a coordinated change in the magnitude of angle α with the speed of rotation. And to cancel the corresponding forces, it is necessary to adjust the speed of rotation, creating a negative torque around the *z* axis. Increasing the accuracy of linearization is possible by eliminating unnecessary opposite forces in the y_b direction.

5. The use of the predictive amplification method in the future makes it possible, albeit by reducing the versatility of the controller, to increase its realism. To improve the functioning of the models, the controller was configured for more realistic output and input parameters. The change in the principles of linearization of the input signal led to it acting more as a trigonometric function of predictive amplification. The result has made it possible to find out the influence of the orientation of ATs on the position of the vessel, and the linearity of the model affects the functionality of the controller.

Conflicts of interest

The authors declare that they have no conflicts of interest in relation to the current research, including financial, personal, authorship, or any other, that could affect the research and the results reported in this paper.

Funding

The research was carried out within the framework of projects of scientific fundamental and applied research and scientific and technical (experimental) developments, which were funded by the Ministry of Education and Science of Ukraine:

– research work "Power plant, propulsion complex, and control system of autonomous sailing apparatus of dual purpose" (State registration number 0120*U*102577;

– research work "Energy efficient positioning system of dual-use vessel" (State registration number 0119*U*001651).

Data availability

The manuscript has linked data in the data warehouse.

References

1. Budashko, V. (2017). Formalization of design for physical model of the azimuth thruster with two degrees of freedom by computational fluid dynamics methods. Eastern-European Journal of Enterprise Technologies, 3 (7 (87)), 40–49. doi: https://doi.org/10.15587/1729-4061.2017.101298

2. Budashko, V., Golikov, V. (2017). Theoretical-applied aspects of the composition of regression models for combined propulsion complexes based on data of experimental research. Eastern-European Journal of Enterprise Technologies, 4 (3 (88)), 11–20. doi: https://doi.org/10.15587/1729-4061.2017.107244

3. Vitalii, B., Vitalii, N., Mark, N., Sergii, K. (2018). Parametrization and identification of energy flows in the ship propulsion complex. 2018 14th International Conference on Advanced Trends in Radioelecrtronics, Telecommunications and Computer Engineering (TCSET). doi: https://doi.org/10.1109/tcset.2018.8336205

4. Budashko, V. V. (2017). Design of the three-level multicriterial strategy of hybrid marine power plant control for a combined propulsion complex. Electrical Engineering & Electromechanics, 2, 62–72. doi: https://doi.org/10.20998/2074-272x.2017.2.10

5. Budashko, V., Nikolskyi, V., Onishchenko, O., Khniunin, S. (2016). Decision support system's concept for design of combined propulsion complexes. Eastern-European Journal of Enterprise Technologies, 3 (8 (81)), 10–21. doi: https://doi.org/10.15587/1729-4061.2016.72543

6. Chen, T.-Y. (2013). An interval-valued intuitionistic fuzzy LINMAP method with inclusion comparison possibilities and hybrid averaging operations for multiple criteria group decision making. Knowledge-Based Systems, 45, 134–146. doi: https://doi.org/10.1016/j.knosys.2013.02.012

7. Fossen, T. I., Sagatun, S. I., Sørensen, A. J. (1996). Identification of dynamically positioned ships. Control Engineering Practice, 4 (3), 369–376. doi: https://doi.org/10.1016/0967-0661(96)00014-7

8. Liang, C. C., Cheng, W. H. (2004). The optimum control of thruster system for dynamically positioned vessels. Ocean Engineering, 31 (1), 97–110. doi: https://doi.org/10.1016/s0029-8018(03)00016-7

9. Uyar, E., Alpkaya, A. T., Mutlu, L. (2016). Dynamic Modelling, Investigation of Manoeuvring Capability and Navigation Control of a Cargo Ship by using Matlab Simulation. IFAC-PapersOnLine, 49 (3), 104–110. doi: https://doi.org/10.1016/j.ifacol.2016.07.018

10. Naeem, W., Sutton, R., Ahmad, S. M. (2003). LQG/LTR Control of an Autonomous Underwater Vehicle Using a Hybrid Guidance Law. IFAC Proceedings Volumes, 36 (4), 31–36. doi: https://doi.org/10.1016/s1474-6670(17)36653-3

11. Skjetne, R., Fossen, T. I., Kokotović, P. V. (2005). Adaptive maneuvering, with experiments, for a model ship in a marine control laboratory. Automatica, 41 (2), 289–298. doi: https://doi.org/10.1016/j.automatica.2004.10.006

12. Ljungberg, F. (2020). Estimation of Nonlinear Greybox Models for Marine Applications. Linköping Studies in Science and Technology. Linköping. doi: https://doi.org/10.3384/lic.diva-165828

13. Lang, X., Mao, W. (2020). A semi-empirical model for ship speed loss prediction at head sea and its validation by full-scale measurements. Ocean Engineering, 209, 107494. doi: https://doi.org/10.1016/j.oceaneng.2020.107494

14. Aurlien, A., Breivik, M., Eriksen, B.-O. H. (2021). Multivariate Modeling and Adaptive Control of Autonomous Ferries. IFAC-PapersOnLine, 54 (16), 395–401. doi: https://doi.org/10.1016/j.ifacol.2021.10.122

15. Sukkarieh, S., Nebot, E. M., Durrant-Whyte, H. F. (1999). A high integrity IMU/GPS navigation loop for autonomous land vehicle applications. IEEE Transactions on Robotics and Automation, 15 (3), 572–578. doi: https://doi.org/10.1109/70.768189

16. Wang, Z., Montanaro, U., Fallah, S., Sorniotti, A., Lenzo, B. (2018). A gain scheduled robust linear quadratic regulator for vehicle direct yaw moment Control. Mechatronics, 51, 31–45. doi: https://doi.org/10.1016/j.mechatronics.2018.01.013

17. Sandler, A., Budashko, V. (2022). Improving tools for diagnosing technical condition of ship electric power installations. Eastern-European Journal of Enterprise Technologies, 5 (5 (119)), 25–33. doi: https://doi.org/10.15587/1729-4061.2022.266267

18. Caron, F., Duflos, E., Pomorski, D., Vanheeghe, P. (2006). GPS/IMU data fusion using multisensor Kalman filtering: introduction of contextual aspects. Information Fusion, 7 (2), 221–230. doi: https://doi.org/10.1016/j.inffus.2004.07.002

19. Ccolque-Churquipa, A., Cutipa-Luque, J. C., Aco-Cardenas, D. Y. (2018). Implementation of a Measurement System for the Attitude, Heading and Position of a USV Using IMUs and GPS. 2018 IEEE ANDESCON. doi: https://doi.org/10.1109/andescon.2018.8564668

20. Chrif, L., Kadda, Z. M. (2014). Aircraft Control System Using LQG and LQR Controller with Optimal Estimation-Kalman Filter Design. Procedia Engineering, 80, 245–257. doi: https://doi.org/10.1016/j.proeng.2014.09.084

21. Budashko, V. V. (2016). Increasing control's efficiency for the ship's two-mass electric drive. Electrical Engineering & Electromechanics, 4, 34–42. doi: https://doi.org/10.20998/2074-272x.2016.4.05

22. Gibson, J. D. (2003). Performance effects of optimal LQG eigenvalue placement in ship control. IECON'03. 29th Annual Conference of the IEEE Industrial Electronics Society (IEEE Cat. No.03CH37468). doi: https://doi.org/10.1109/iecon.2003.1279991

23. Jerrelind E. (2021). Linear Quadratic Control of a Marine Vehicle with Azimuth Propulsion, Internet, Dissertation. Available from: http://urn.kb.se/resolve?urn=urn:nbn:se:liu:diva-178007

24. Sir Elkhatem, A., Naci Engin, S. (2022). Robust LQR and LQR-PI control strategies based on adaptive weighting matrix selection for a UAV position and attitude tracking control. Alexandria Engineering Journal, 61 (8), 6275–6292. doi: https://doi.org/10.1016/j.aej.2021.11.057

25. Gandhi, P., Adarsh, S., Ramachandran, K. I. (2017). Performance Analysis of Half Car Suspension Model with 4 DOF using PID, LQR, FUZZY and ANFIS Controllers. Procedia Computer Science, 115, 2–13. doi: https://doi.org/10.1016/j.procs.2017.09.070

26. Linder, J. (2014). Graybox Modelling of Ships Using Indirect Input Measurements. Linköping. doi: https://doi.org/10.3384/lic.diva-111095

27. Oosterveld, M. W. C., van Oossanen, P. (1975). Further computer-analyzed data of the Wageningen B-screw series. International Shipbuilding Progress, 22 (251), 251–262. doi: https://doi.org/10.3233/isp-1975-2225102

28. Sáez, D., Cipriano, A. (1998). Fuzzy Linear Quadratic Regulator Applied to the Real Time Control of an Inverted Pendulum. IFAC Proceedings Volumes, 31 (4), 155–160. doi: https://doi.org/10.1016/s1474-6670(17)42150-1

29. Sørensen, A. J., Ådnanes, A. (1997). High Performance Thrust Allocation Scheme in Positioning of Ships Based on Power and Torque Control. Marine Technology Society. Available at: https://www.researchgate.net/publication/255649795_High_Performance_Thrust_Allocation_Scheme_in_Positioning_of_Ships_Based_on_Power_and_Torque_Control

30. Myrhorod, V., Hvozdeva, I., Budashko, V. (2020). Multi-parameter Diagnostic Model of the Technical Conditions Changes of Ship Diesel Generator Sets. 2020 IEEE Problems of Automated Electrodrive. Theory and Practice (PAEP). doi: https://doi.org/10.1109/paep49887.2020.9240905

31. Budashko, V., Shevchenko, V. (2021). The synthesis of control system to synchronize ship generator assemblies. Eastern-European Journal of Enterprise Technologies, 1 (2 (109)), 45–63. doi: https://doi.org/10.15587/1729-4061.2021.225517

32. Zanchetta, M., Tavernini, D., Sorniotti, A., Gruber, P., Lenzo, B., Ferrara, A. et al. (2019). Trailer control through vehicle yaw moment control: Theoretical analysis and experimental assessment. Mechatronics, 64, 102282. doi: https://doi.org/10.1016/j.mechatronics.2019.102282

33. Budashko, V., Shevchenko, V. (2018). Synthesis of the Management Strategy of the Ship Power Plant for the Combined Propulsion Complex. 2018 IEEE 5th International Conference on Methods and Systems of Navigation and Motion Control (MSNMC). doi: https://doi.org/10.1109/msnmc.2018.8576266

34. Hvozdeva, I., Myrhorod, V., Budashko, V., Shevchenko, V. (2020). Problems of Improving the Diagnostic Systems of Marine Diesel Generator Sets. 2020 IEEE 15th International Conference on Advanced Trends in Radioelectronics, Telecommunications and Computer Engineering (TCSET). doi: https://doi.org/10.1109/tcset49122.2020.235453

35. Budashko, V. (2020). Thrusters Physical Model Formalization with regard to Situational and Identification Factors of Motion Modes. 2020 International Conference on Electrical, Communication, and Computer Engineering (ICECCE). doi: https://doi.org/10.1109/icecce49384.2020.9179301

36. Wu, T.-S., Karkoub, M., Yu, W.-S., Chen, C.-T., Her, M.-G., Wu, K.-W. (2016). Anti-sway tracking control of tower cranes with delayed uncertainty using a robust adaptive fuzzy control. Fuzzy Sets and Systems, 290, 118–137. doi: https://doi.org/10.1016/j.fss.2015.01.010

37. Sandler, A. K., Budashko, V. V. (2022). Volokonno-optychnyi inklinometr dlia diahnostuvannia elementiv sudnovoho propulsyvnoho kompleksu. XI naukova konferentsiya «Naukovi pidsumky 2022 roku». Kharkiv: Tekhnolohichnyi tsentr, 43–44. Available at: https://entc.com.ua/download/Збірник%20тез_11_Наукової%20конференції_НАУКОВІ%20ПІДСУМКИ%202022%20РОКУ_.pdf

38. Budashko, V., Shevchenko, V. (2021). Solving a task of coordinated control over a ship automated electric power system under a changing load. Eastern-European Journal of Enterprise Technologies, 2 (2 (110)), 54–70. doi: https://doi.org/10.15587/1729-4061.2021.229033

39. Budashko, V., Sandler, A., Shevchenko, V. (2022). Optimization of the control system for an electric power system operating on a constant-power hyperbole. Eastern-European Journal of Enterprise Technologies, 1 (8 (115)), 6–17. doi: https://doi.org/10.15587/1729-4061.2022.252172

40. Budashko, V., Sandler, A., Shevchenko, V. (2022). Diagnosis of the Technical Condition of High-tech Complexes by Probabilistic Methods. TransNav, the International Journal on Marine Navigation and Safety of Sea Transportation, 16 (1), 105–111. doi: https://doi.org/10.12716/1001.16.01.11

41. Myrhorod, V., Gvozdeva, I., Budashko, V. (2022). Approximation - markov models of changes in the technical condition parameters of power and energy installations in long-term operation. Aerospace Technic and Technology, 4sup2, 73–79. doi: https://doi.org/10.32620/aktt.2022.4sup2.11

42. Hvozdeva, I. M., Myrhorod, V. F., Budasko, V. V. (2021). Two-dimensional singular decomposition of time series components. Applied Questions of Mathematical Modeling, 4, 66–75. doi: https://doi.org/10.32782/kntu2618-0340/2021.4.2.1.6